Stem Cell Reports
Resource
ISSCR
OPEN ACCESS

Purification of human iPSC-derived cells at large scale using microRNA switch and magnetic-activated cell sorting

Yuta Tsujisaka,[1,2,5] Takeshi Hatani,[1,2,5] Chikako Okubo,[1] Ryo Ito,[1] Azuma Kimura,[1] Megumi Narita,[1] Kazuhisa Chonabayashi,[1,3] Shunsuke Funakoshi,[1,4] Antonio Lucena-Cacace,[1] Taro Toyoda,[1] Kenji Osafune,[1] Takeshi Kimura,[2] Hirohide Saito,[1,*] and Yoshinori Yoshida[1,4,*]

[1]Center for iPS Cell Research and Application, Kyoto University, Kyoto 606-8507, Japan
[2]Department of Cardiovascular Medicine, Graduate School of Medicine, Kyoto University, Kyoto 606-8507, Japan
[3]Department of Hematology and Oncology, Graduate School of Medicine, Kyoto University, Kyoto 606-8507, Japan
[4]Takeda-CiRA Joint Program (T-CiRA), Fujisawa 251-0012, Japan
[5]These authors contributed equally
*Correspondence: hirohide.saito@cira.kyoto-u.ac.jp (H.S.), yoshinor@cira.kyoto-u.ac.jp (Y.Y.)
https://doi.org/10.1016/j.stemcr.2022.05.003

SUMMARY

For regenerative cell therapies using pluripotent stem cell (PSC)-derived cells, large quantities of purified cells are required. Magnetic-activated cell sorting (MACS) is a powerful approach to collect target antigen-positive cells; however, it remains a challenge to purify various cell types efficiently at large scale without using antibodies specific to the desired cell type. Here we develop a technology that combines microRNA (miRNA)-responsive mRNA switch (miR-switch) with MACS (miR-switch-MACS) to purify large amounts of PSC-derived cells rapidly and effectively. We designed miR-switches that detect specific miRNAs expressed in target cells and controlled the translation of a CD4-coding transgene as a selection marker for MACS. For the large-scale purification of induced PSC-derived cardiomyocytes (iPSC-CMs), we transferred miR-208a-CD4 switch-MACS and obtained purified iPSC-CMs efficiently. Moreover, miR-375-CD4 switch-MACS highly purified pancreatic insulin-producing cells and their progenitors expressing Chromogranin A. Overall, the miR-switch-MACS method can efficiently purify target PSC-derived cells for cell replacement therapy.

INTRODUCTION

Cardiovascular diseases are the leading cause of morbidity and mortality in the world (Virani et al., 2020). To overcome cardiovascular diseases, strenuous efforts to develop new therapies are being made both at the experimental and clinical levels (Sanganalmath and Bolli, 2013). Cardiac replacement therapy using cardiomyocytes (CMs) differentiated from pluripotent stem cells (PSCs), including embryonic stem cells and induced PSCs (iPSCs) have shown many beneficial effects to infarcted hearts in animal models (Chong et al., 2014; Hatani et al., 2018a; Shiba et al., 2016). However, for the clinical application of PSC-derived CMs (PSC-CMs), 1×10^8–1×10^9 purified PSC-CMs are required (Chong et al., 2014; Hattori and Fukuda, 2012; Shiba et al., 2016). Additionally, the contamination of non-CMs, especially undifferentiated cells, may cause unexpected contingencies and should be avoided. Although cell sorting using a flow cytometer with antibodies against specific cell surface proteins is one promising strategy (Dubois et al., 2011; Osborn et al., 1989), it is time consuming to collect the cells, specific cell surface markers are needed, and contamination of the antibodies on the target cell surface risks an immunogenic reaction and local inflammation after the transplantation, which may lead to graft failure (Dunn et al., 2011).

Magnetic-activated cell sorting (MACS) technology enables time-efficient cell isolation and sorts greater amounts of cells in a shorter time compared with flow cytometers. However, this technology also requires specific antibodies against cell surface proteins and is difficult to apply to cell types that do not have specific cell surface proteins, such as CMs and pancreatic insulin-producing cells.

MicroRNAs (miRNAs) are a class of small non-coding RNAs that regulate gene expressions at the posttranscriptional level by cleaving or translationally repressing their target mRNAs (Ambros, 2001; Bartel, 2004; Nakanishi and Saito, 2019). We previously designed a miRNA-responsive, synthetic mRNA encoding a fluorescent reporter protein and complementary sequences against target miRNA, a technology we call miRNA switch (miR-switch) (Figure 1A) (Miki et al., 2015; Endo et al., 2016; Ohno et al., 2020). This technology changes the translation efficiency of the reporter proteins depending on the expression of the target miRNA in the transfected cells through the hybridization of the synthetic mRNA with the endogenous target miRNA (Figure 1B). Taking advantage of this differential translation, the miR-switch can separate and sort target cells from heterogeneous cell populations using a flow cytometer. We demonstrated that the miR-208a switch specifically separates iPSC-CMs from iPSC-non-CMs with a purity of more than 95% based on troponin T expression. Importantly, the miR-switch degrades in a short time and has no risk of genomic modification, which enables the maintenance of normal gene expressions and miRNA profiles before and after miR-switch transfection

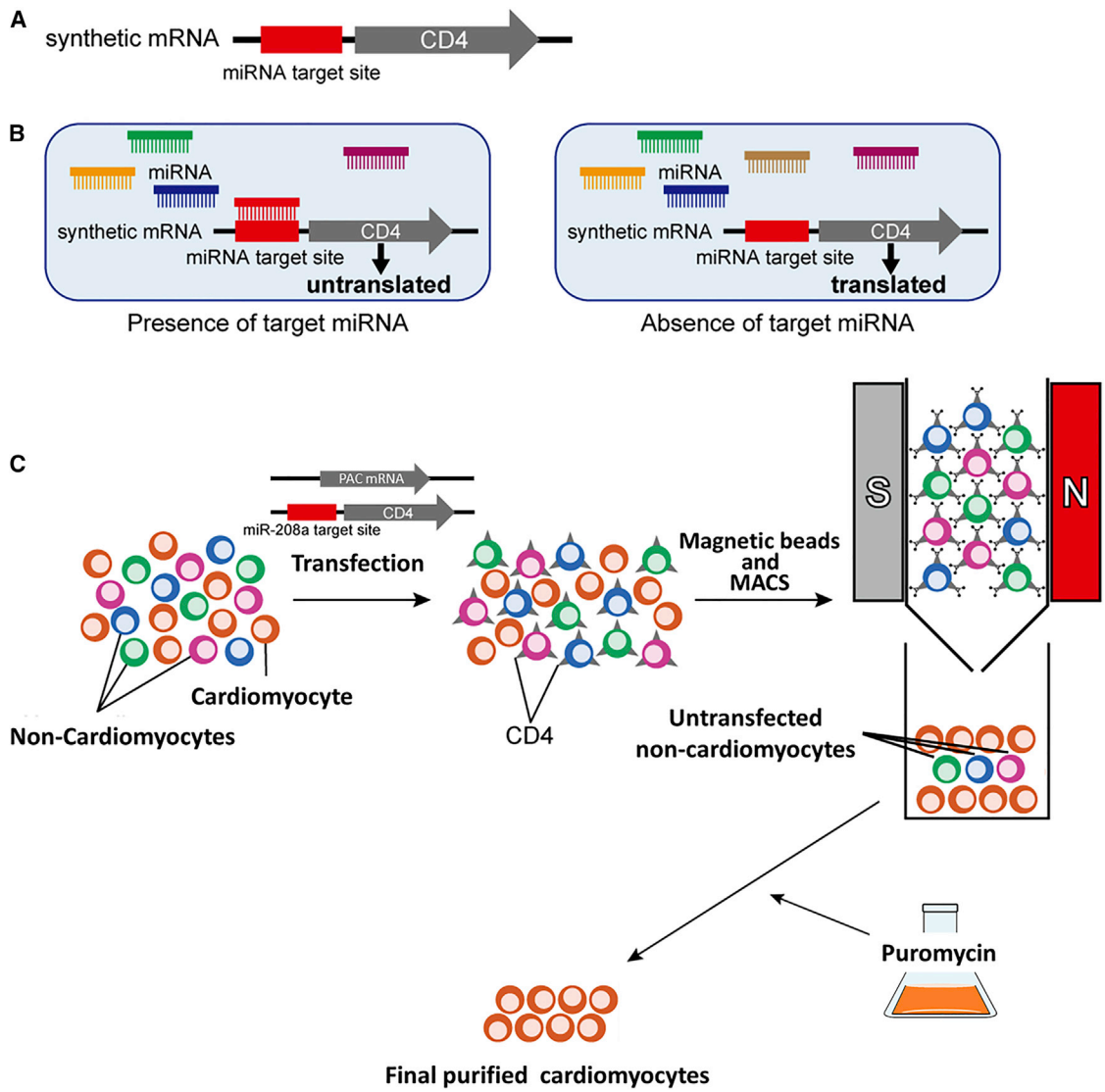

Figure 1. Schematic illustration of this study

(A) The miR-switch is synthetic mRNA made of two parts. One is the miRNA target site, which is a complementary sequence to the target miRNA, and the other is a protein coding sequence. In this study, CD4 was used as the protein for the selection marker in MACS.

(B) After the transfection of the miR-switch, if the cell expresses the target miRNA, translation from the miR-switch is inhibited, due to the interaction between the miRNA and the miR-switch. In contrast, if the cell does not express the target miRNA, the miR-switch is translated.

(C) Thus, upon transfecting miR-208a-CD4-switch to a heterogeneous cell population, CD4 translation is inhibited in CMs, but not in other cell types. Using CD4 microbeads and MACS, non-CMs bind to the MACS column, and CMs are isolated. By co-transfecting *PAC* mRNA, untransfected non-CMs are removed after puromycin administration.

(Miki et al., 2015). Thus, miR-switch technology has the potential for clinical application, but its combination with flow cytometric cell sorting is not suitable for collecting a large number of cells in a short time, a condition required in regenerative medicine.

Therefore, in this study, we developed a novel purification method of human iPSC-derived cells at large scale by combining the miR-switch and MACS (miR-switch-MACS). We designed miR-switches that encode the CD4 cell surface protein and contain complementary sequences against the target miRNA. The combination of the miR-switch-MACS using microbeads conjugated to monoclonal anti-human CD4 antibody enabled the large-scale purification of iPSC-CMs efficiently, without the attachment of the

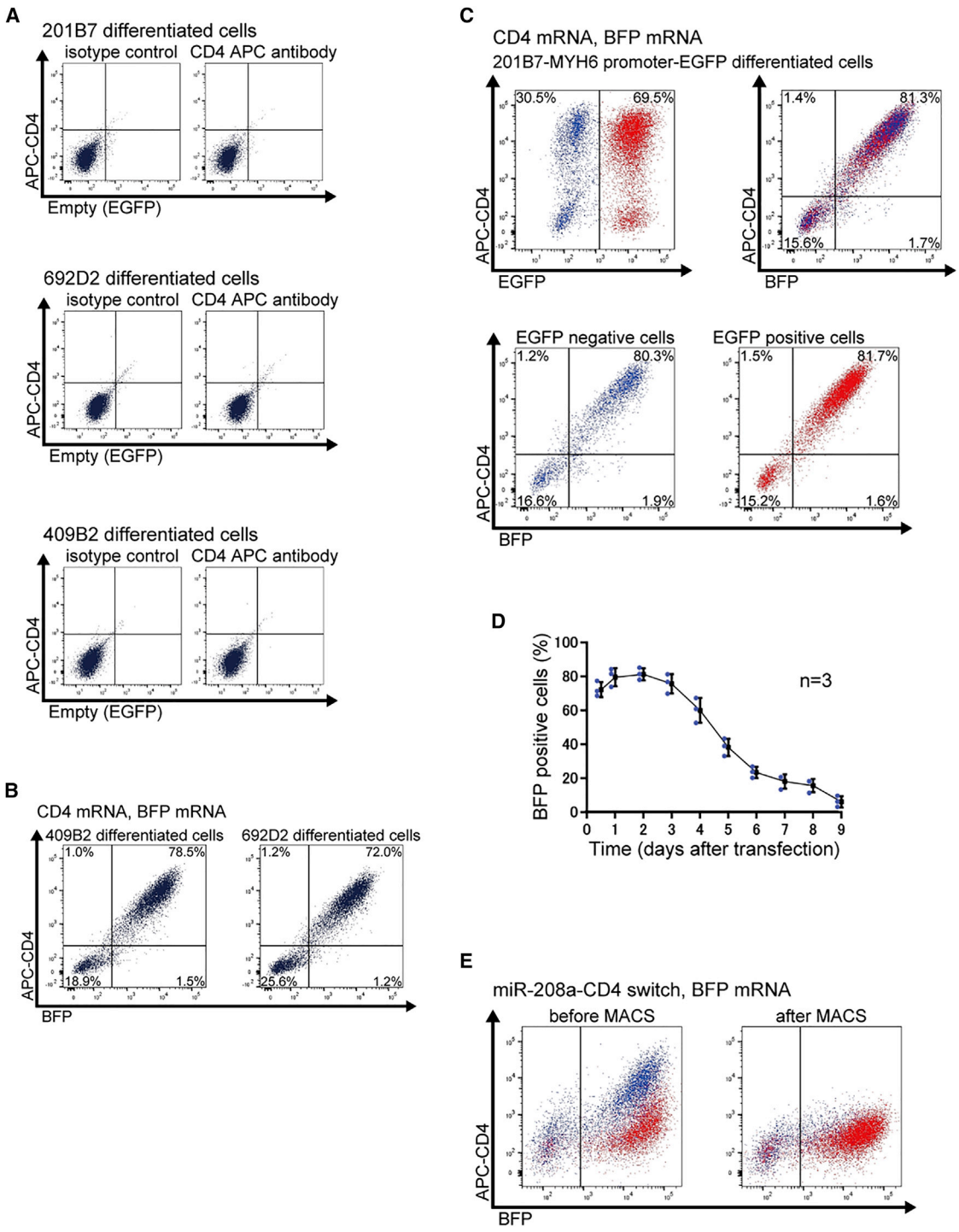

Figure 2. CD4 mRNA and miR-208a-CD4-switch transfection in differentiated cells

(A) Differentiated 201B7, 409B2, and 692D2 iPSCs showed no CD4 expression on the cell surface. Representative data from two biologically independent experiments are shown.

(B) Co-transfection of CD4 mRNA and BFP mRNA to differentiated 409B2 and 692D2 iPSCs. Representative data from two biologically independent experiments are shown. In the left panel, BFP expression was 80.0%, and CD4 expression was 79.5%. In the right panel, the percentages were 73.2 and 73.2%, respectively.

(legend continued on next page)

antibody on the target cell (Figure 1C). We engrafted human iPSC-CMs purified by this method in a mouse model of acute myocardial infarction. Moreover, we also showed that insulin-producing pancreatic progenitor cells (chromogranin A-positive cells) could be purified using miR-375-CD4 switch-MACS. These data indicate that miR-switch-MACS technology can be applied to cell therapies that require large-scale cell preparation.

RESULTS

Transfection of CD4-encoding mRNA to iPSC-derived cells

We aimed to purify iPSC-CMs by removing non-CMs ectopically expressing a cell surface protein (Figure 1C). We first differentiated iPSCs into iPSC-CMs, and, by flow cytometry, investigated the expressions of CD4 and CD271 in differentiated cells, including iPSC-CMs, because MACS antibodies against CD4 and CD271 are available commercially. Some differentiated cells from 201B7 iPSCs expressed CD271 (Figure S1), but none differentiated from three different iPSC lines (201B7, 409B2, and 692D2) expressed CD4 (Figure 2A). Because differentiated cells should not express the surface protein endogenously, we selected CD4 for the following experiments. After the co-transfection of two mRNAs coding for CD4 and *BFP*, we found these proteins were expressed efficiently at a similar level (Figure 2B). We then compared the expression level of CD4 in CMs (GFP positive) and non-CMs (GFP negative) differentiated from the cardiac iPSC reporter line 201B7-MYH6-EGFP (Funakoshi et al., 2016). We found similar CD4 expression levels between GFP positive and GFP-negative cells, indicating that mRNA can be transfected and translated in both CM and non-CM populations (Figure 2C). We also assessed the time course of the protein expression of *BFP*, finding transfected *BFP* mRNA expression was high in the first 3 days, but decreased gradually thereafter, and fell to less than one-half within 5 days (Figure 2D and Table S1).

Transfection of miR-208a-CD4 switch

Next, we investigated whether we could modulate ectopic CD4 expression levels by the endogenous and specific miRNA expression in iPSC-CMs. As a marker for CM-specific miRNA, we chose miR-208a, because the fluorescent protein expression difference between CMs and non-CMs was largest using the miR-208a switch (Miki et al., 2015). Thus, we designed miR-208a-responsive CD4-coding mRNA (miR-208a-CD4 switch) to selectively repress CD4 expression in iPSC-CMs. We transfected different amounts of miR-208a-CD4 switch (100, 200, 300, 600, and 900 ng) and 300 ng of control *BFP* mRNA to 201B7-MYH6-EGFP-differentiated cells and compared expression profiles (Figure S2 and Table S2). Flow cytometric analysis showed the CD4 signal intensity of iPSC-CMs and non-iPSC-CMs increased with higher quantities of transfected miR-208a-CD4 switch. After MACS, CD4-positive cells were clearly eliminated. We used 300 ng miR-208a-CD4 switch to collect large quantities of iPSC-CMs, because we could efficiently purify iPSC-CMs among transfected cells (>95% purity), and retain more than 50% of iPSC-CMs based on the calculation of the number of CMs before and after MACS (Figures 2E, S2, and Table S2).

Purification of iPSC-CMs with miR-208a switch-MACS

Since untransfected cells do not express CD4, the cells sorted by MACS still contained untransfected cells. To eliminate these cells, we co-transfected miR-208a-CD4 switch and puromycin N-acetyltransferase (*PAC*) mRNA instead of *BFP* mRNA (Figure 3A). Flow cytometric analysis using an antibody against troponin T revealed that iPSC-CMs were highly purified after MACS and the subsequent 48 h administration of puromycin (Figures 3B, 3C, and Table S3). Indeed, we found that iPSC-CMs were purified at more than 97% in three different iPSC lines. Immunostaining also showed that iPSC-CMs were highly purified (Figure 3D). In addition, purified iPSC-CMs spontaneously beat and were characterized by ventricular action potentials having a long plateau phase and a typical action potential duration (APD) ratio (APD90/APD50 < 1.4)

(C) Co-transfection of CD4 mRNA and BFP mRNA to differentiated 201B7-MYH6-EGFP iPSCs. Representative data from two biologically independent experiments are shown. EGFP-positive cells, which are CMs, were 69.5% of the cell population (red). EGFP-negative cells, which are non-CMs, were 30.5% of the cell population (blue). In the upper right panel, BFP expression was 83.0% and CD4 expression was 82.7%. In the lower panel, BFP expression was 82.2% and CD4 expression was 81.5% in EGFP negative cells and 83.3 and 83.2%, respectively, in EGFP positive cells.

(D) Time course of the mRNA expression as assessed by the flow cytometric analysis of BFP-positive cells from 12 h to 9 days after the transfection of 201B7 differentiated cells. The values were acquired from three biologically independent measurements. The actual values are shown in Table S1.

(E) Transfection of 300 ng of miR-208a-CD4 switch to differentiated 201B7-MYH6-EGFP iPSCs. Representative data from three biologically independent experiments are shown. Red shows EGFP-positive cells (CMs) and blue shows EGFP-negative cells (non-CMs). The analysis before MACS is shown in the left panel, and the analysis after MACS is shown in the right panel. After MACS sorting, CD4-positive cells were eliminated.

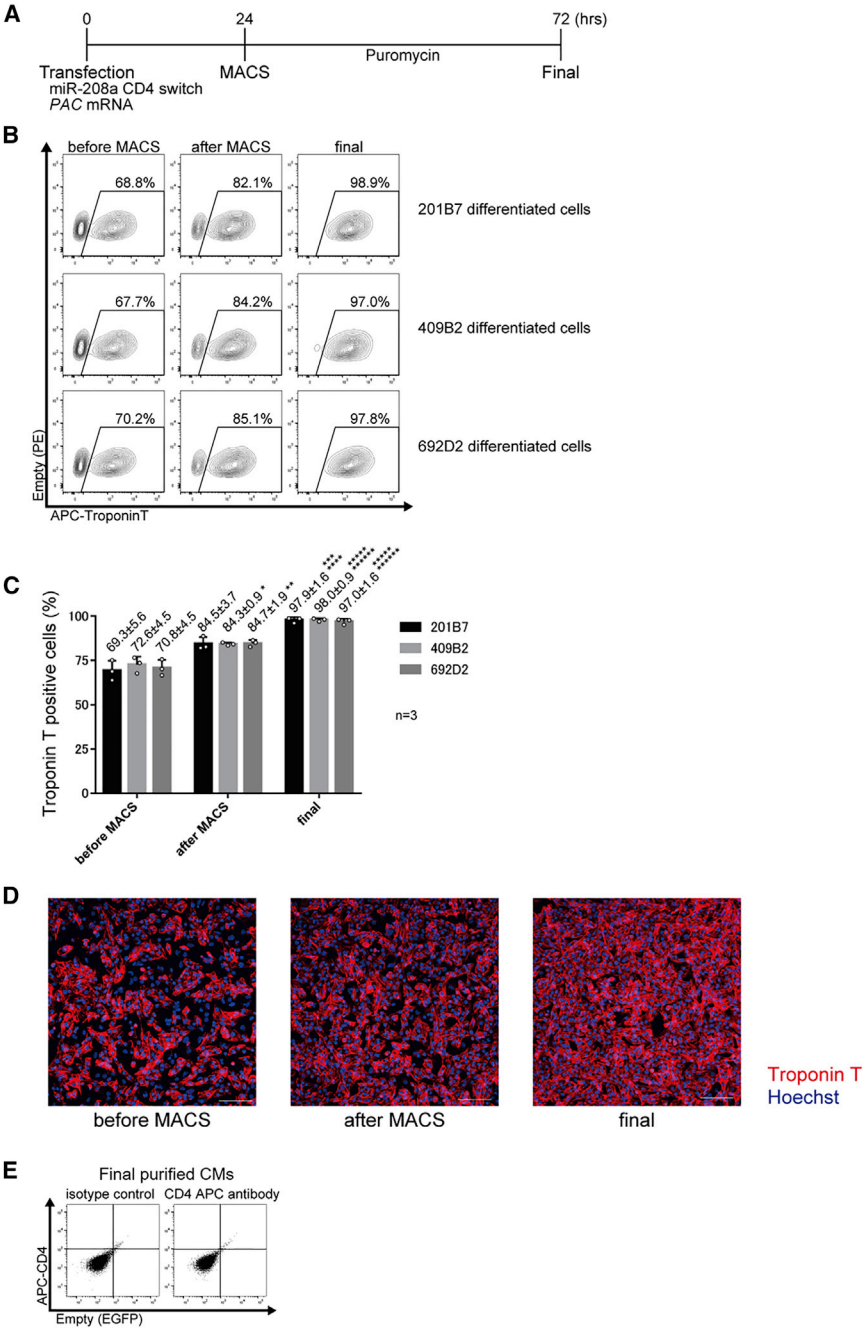

Figure 3. Purification of iPSC-CMs using miR-208a-CD4 switch and MACS

(A) Schematic procedure for the purification of iPSC-CMs using miR-208a-CD4 switch and MACS. To eliminate untransfected cells, *PAC* mRNA and puromycin were used.

(B) Representative data of troponin T-positive differentiated 201B7, 409B2, and 692D2 iPSCs before MACS, after MACS, and after purification with puromycin (final). Representative data are shown from three biologically independent experiments. The boxed areas indicate troponin T-positive cells.

(C) The percentage of troponin T-positive differentiated 201B7, 409B2, and 692D2 iPSCs before MACS, after MACS, and after purification. The values are from three biologically independent measurements and denoted as mean ± standard deviation. *p < 0.015 versus the corresponding sample before MACS, **p < 0.01 versus the corresponding sample before MACS, ***p < 0.005 versus the corresponding sample after MACS, ****p < 0.005 versus the corresponding sample before MACS, *****p < 0.001 versus the corresponding sample after MACS, ******p < 0.001 versus the corresponding sample before MACS. The data were analyzed by the Bonferroni-Dunn test. Actual values are shown in Table S3.

(D) Fluorescence immunostaining of differentiated 201B7 iPSCs before MACS, after MACS, and after the final purification (n = 3). Representative data from three biologically independent experiments are shown. Red, troponin T; blue, Hoechst. Scale bars, 100 μm.

(E) CD4 expression of the final purified CMs using the miR-208a switch-MACS method. Flow cytometric analysis found no CD4 expression in the final purified CMs after application of the miR-208a-CD4 MACS method and subsequent 48 h administration of puromycin.

(Burridge et al., 2014) (Figure S3A and Table S4). We also confirmed that the final purified iPSC-CM population did not express CD4, indicating that transfected miR-208a-CD4 switch in iPSC-CMs did not induce the translation of CD4 after MACS (Figure 3E).

RNA expression analysis of purified iPSC-CMs

Next, we compared the gene expression profiles of the iPSC-CMs purified by the miR-switch-MACS method and those sorted by a conventional antibody-based method (CD172a/b positive, CD31 negative, CD49a negative, CD90 negative, and CD140b negative). Hierarchical clustering analysis of the samples revealed that iPSC-CMs induced in the first experiment (lot #1) and iPSC-CMs induced in the second experiment (lot #2) were classified in the same clustering, indicating differences in the expression profiles of the iPSC-CMs sorted by the two methods were smaller than those between the two lots

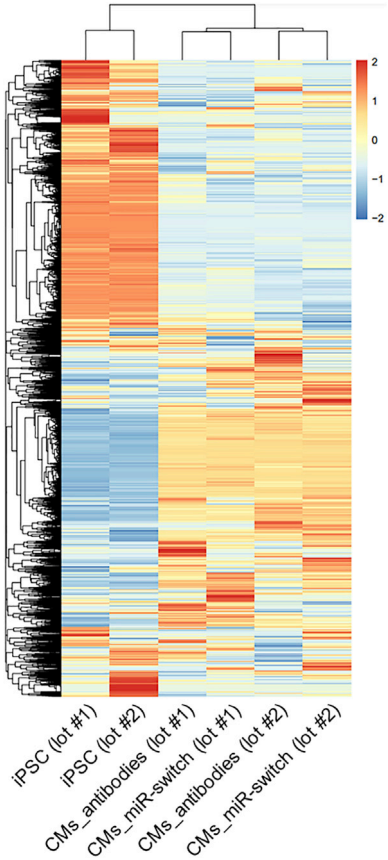

Figure 4. Hierarchical clustering of gene expression profiles

Hierarchical clustering of the gene expression profiles of 201B7 iPSCs (control), 201B7 iPSC-CMs purified by antibodies (CD172a/b positive, CD31 negative, CD49a negative, CD90 negative, and CD140b negative), and 201B7 iPSC-CMs purified by the miR-208a-CD4-switch and MACS. The data are shown from two biologically independent experiments. Color indicates scaled values of log2 (normalized counts).

(Figure 4). These data suggest that the cellular characteristics of iPSC-CMs purified by the miR-switch-MACS method are similar to those purified by the conventional method.

Transplantation of purified iPSC-CMs

We next investigated the viability of the sorted iPSC-CMs *in vivo*. We differentiated iPSC-CMs from 201B7-luc iPSCs (Funakoshi et al., 2016) and purified them using the miR-switch-MACS method. Thereafter, we transplanted the cells by direct injection into immunodeficient NOG mouse hearts with myocardial infarction. Hearts were extracted from the mice three months after the transplantation and fixed with 4% paraformaldehyde in PBS. Immunostaining against troponin T and luciferase confirmed that 201B7-luc iPSC-CMs purified using the miR-switch-MACS method were engrafted efficiently and substantially in the mouse heart (Figure 5). High-magnification images revealed that the transplanted iPSC-CMs formed sarcomere structures (Figure S4A).

Echocardiography showed that left ventricular diastolic dimensions (LVDd) and left ventricular systolic dimensions (LVDs) were increased and the fractional shortening (FS) was decreased just after the myocardial infarction in both groups. However, at 1 week after the injection, the FS was significantly higher in the transplanted group compared with the control. Similarly, the LVDd at 2 weeks after the injection was significantly lower in the transplanted group. These differences were maintained for the 3-month follow-up period. Thus, LV remodeling and reduced LV function after the myocardial infarction were relatively mild in mice with transplanted iPSC-CMs compared with control mice, and the cardiac function was significantly better with iPSC-CM transplantation (Figure S4B).

Collectively, iPSC-CMs purified by the miR-208a switch-MACS method could engraft *in vivo* and improved cardiac function, suggesting the versatility for regenerative cell transplantation therapy.

Time and efficiency for the purification of iPSC-CMs

To compare the time efficiency of the miR-switch-MACS method and conventional antibody-based flow cytometric cell sorting, we measured the time to obtain a large scale of purified iPSC-CMs. We finally obtained $1.85 \pm 0.14 \times 10^8$ purified cells after 28 min of MACS and the following 48 h of puromycin administration. In contrast, we obtained only $1.15 \pm 0.042 \times 10^6$ purified cells after 27 min of fluorescence-activated cell sorting (FACS) (Table S5). Based on these results, we assume that FACS would take approximately 68 h to obtain the equal amount of the final purified cells using miR-switch-MACS method. In contrast, although the miR-switch-MACS method requires the additional 48 h of puromycin selection, it does not require continuous FACS runs. Thus, the miR-switch-MACS method is a highly efficient and simple approach compared with FACS-based methods.

To bypass the flow cytometric cell sorting process, in our previous work, we used Bim as another reporter of miR-switch and demonstrated that miR-208a-Bim induced apoptosis selectively in non-iPSC-CMs to purify the iPSC-CM population, although the purification efficiency of iPSC-CMs was approximately 90% (Miki et al., 2015). Here we compared the efficiency of miR-208a-Bim and miR-208a-CD4 by transfecting both of them. The miR-208a-CD4 switch resulted in a significantly higher purity than the miR-208a-Bim switch ($p < 0.001$, by two-way ANOVA with repeated measures) (Figure S5 and Table S6).

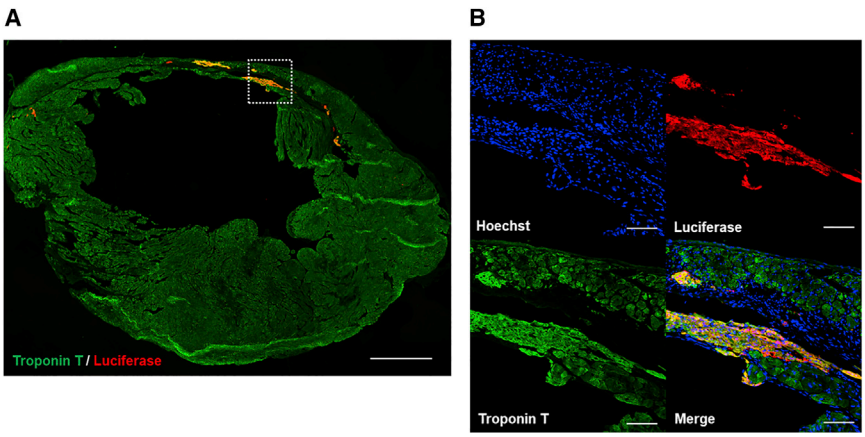

Figure 5. Engraftment of iPSC-CMs purified using the miR-208a switch-MACS method

Anti-luciferase immunostaining (red) demonstrated that a substantial amount of iPSC-CMs was engrafted in the host mouse left ventricular wall with myocardial infarction three months after the transplantation. Representative data are shown from nine biologically independent experiments. Immunostaining of troponin T (green) marks CMs.

(A) The relatively thin anterior wall of the LV indicates an infarcted area. Scale bar, 1000 μm.

(B) A high magnification of the region of interest indicated by the white square in (A). The troponin T-negative area indicates the scar of the myocardial infarction. Scale bars, 100 μm.

Purification of subtype-specific iPSC-CMs with miR-208a switch

To investigate further application of the miR-208a switch-MACS method, we transfected miR-208a switch into cells differentiated from iPSCs using CM subtype-specific protocols.

Our standard iPSC differentiation protocol favors the development of ventricular iPSC-CMs (ventricular protocol). To confirm this, we differentiated 201B7 iPSCs, purified them using miR-208a switch, and immunostained the final cell product with antibodies against troponin T and MLC2V, which is a ventricular-specific myosin isoform. Immunostaining showed that almost all cells were troponin T positive and MLC2V positive (Figure 6A). Next, we differentiated 201B7 iPSCs using the atrial protocol and purified them as above. Before purification, the percentage of troponin T positive cells and the percentage of cells that reacted to miR-208a switch were similar (Figure 6B). Moreover, flow cytometric analysis after the purification showed that the percentage of troponin T-positive cells was approximately 95% (95.4 ± 3.3%) (Figure 6B). These findings suggest that a high purification of iPSC-CMs was achieved in the atrial protocol as well. Thereafter, we differentiated iPSC-CMs using both protocols. A qPCR analysis of the differentiated cells before purification showed that ventricular-related genes (MYL2 and IRX4) were expressed at significantly higher levels when using the ventricular protocol compared with the atrial protocol. The converse was true for atrial-related genes (COUPTF-II and MYL7). These gene expression differences were maintained in the final purified cell population by the miR-208a switch method as well as the conventional antibody-based method (CD172a/b positive, CD31 negative, CD49a negative, CD90 negative, and CD140b negative) (Figure 6C). Immunostaining of the final purified cell population using both protocols confirmed these differences (ventricular CMs, COUPTF-II negative; atrial CMs, COUPTF-II positive) (Figure 6D). The final purified iPSC-CMs with the atrial protocol spontaneously beat and were characterized by atrial action potentials having absence of a prominent plateau phase and a typical APD ratio (APD90/APD50 > 1.7) (Burridge et al., 2014) (Figure S3B and Table S4).These findings revealed that the miR-208a switch method is capable of purifying atrial iPSC-CMs.

Next, we compared the nodal and ventricular protocols by flow cytometric analysis, qPCR, and immunostaining. Before purification, the percentage of cells reacting to the miR-208a switch was similar with that of troponin T-positive cells. After the purification, 95.2 ± 2.4% of the final purified cell population was troponin T positive (Figure 6E), confirming a high purification of iPSC-CMs when using the nodal protocol. Compared with the ventricular protocol, the differentiated cells from the nodal protocol had a significantly lower expression of ventricular-related genes (MYL2 and IRX4) and significantly higher expression of nodal-related genes (SHOX2 and ISL1). These gene expression profiles were similar after purification using the miR-208a-switch method and the conventional antibody-based method (Figure 6F). In the nodal protocol, immunostaining showed that most of the final purified cell populations were troponin T positive and NKX2.5 negative, which is characteristic of nodal CMs. In contrast, using the ventricular protocol, most of the cells were troponin T positive and NKX2.5 positive, which is characteristic of ventricular CMs (Figure 6G). The final purified iPSC-CMs spontaneously beat relatively faster than those

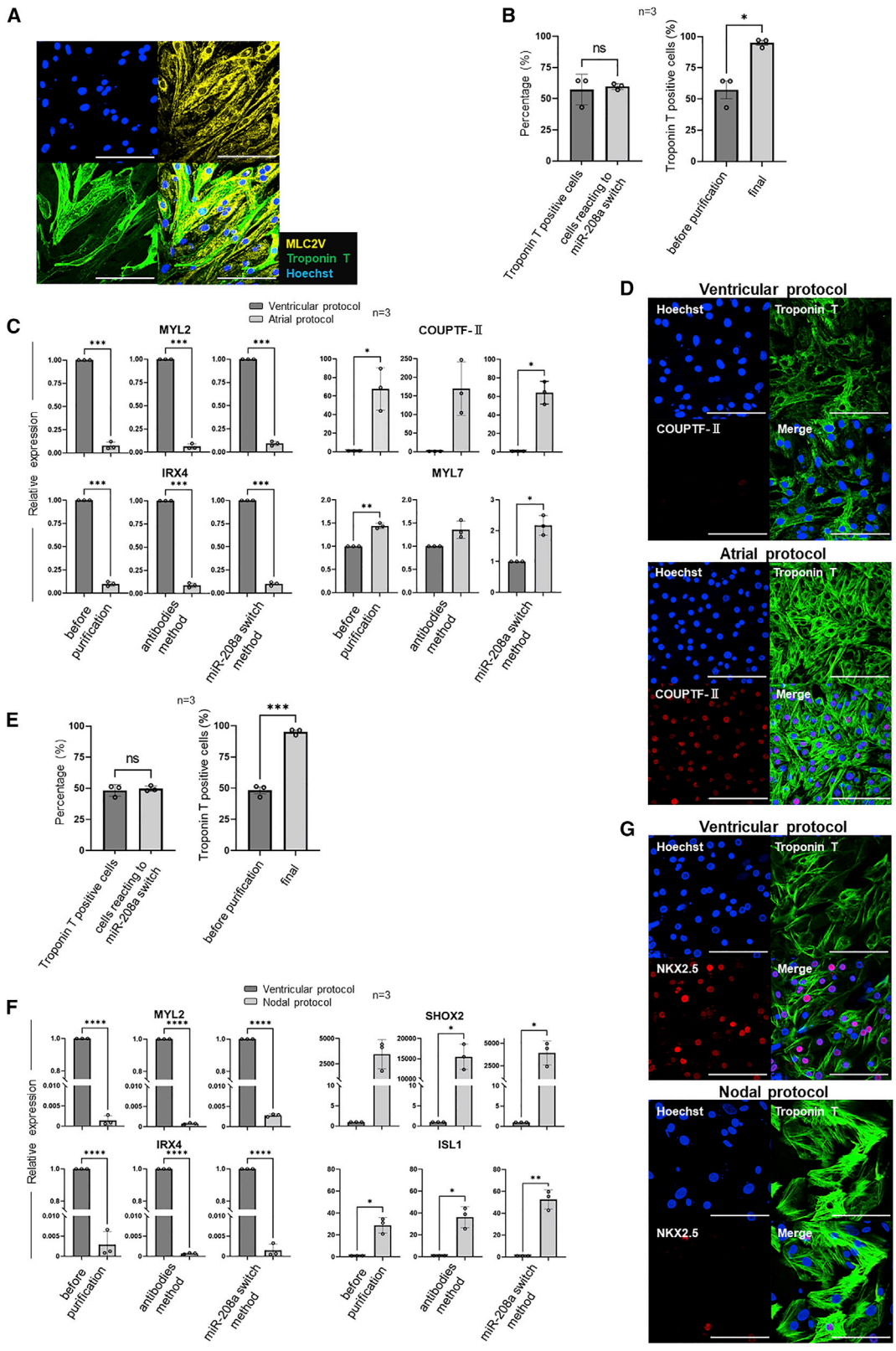

(legend on next page)

using the ventricular and atrial protocols. Nodal action potentials with slow upstroke, prominent phase four depolarization, and a typical APD ratio (1.4 < APD90/APD50 < 1.7) (Burridge et al., 2014) were recorded (Figure S3C and Table S4). Hence, nodal iPSC-CMs can also be purified using the miR-208a-switch method.

Purification of insulin-producing cells with miR-375 switch

Finally, to show the versatility of the miR-switch-MACS method, we aimed to purify and collect other types of cells. We chose miR-375, an insulin-producing cell-expressing miRNA, to collect insulin-producing cells. We transfected miR-375-CD4 switch and *BFP* mRNA simultaneously into differentiated cells derived from iPSCs (585A1) and confirmed that CD4-positive cells were eliminated using MACS (Figure 7A). Next, we co-transfected miR-375-CD4-switch and *PAC* mRNA instead of *BFP* mRNA for purification. Flow cytometric analysis using antibodies against chromogranin A, a marker for pancreatic endocrine precursor cells, and C-peptide showed insulin-producing cells were highly purified after MACS and puromycin selection (Figures 7B, 7C, and Table S7). Immunostaining showed that the final purified cell population included C-peptide positive-cells, glucagon positive cells, and some somatostatin positive cells (Figure 7D). Furthermore, some of the C-peptide positive cells were also positive for PDX1, a marker for functional β cells, suggesting the final purified cell population were fetal-type endocrine cells, including immature β cells.

DISCUSSION

In the present study, we developed a novel and efficient purification method for iPSC-CMs and insulin-producing cells that is applicable to large-scale cell preparation by combining miR-switch-MACS technologies.

Although antibody-based purification methods for CMs using a cell sorter is one promising strategy to prepare the cells for regenerative medicine, this approach is time consuming when collecting the large number of cells needed for cell transplantation. A comparison of the time to purify iPSC-CMs showed that the miR-switch-MACS method could obtain at least 100 times more iPSC-CMs than the conventional cell sorting method using antibodies, despite similar procedure times (Table S5). Even including the subsequent 48 h for puromycin selection after MACS (Figure 3A), the miR-switch-MACS method notably decreases the time and effort needed for standard cell sorting methods. Furthermore, conventional antibody-based purification methods risk contaminating antibodies, which may cause an immunogenic reaction and local inflammation, resulting in graft failure (Dubois et al., 2011; Osborn et al., 1989). In the miR-switch-MACS method, there is the possibility that the low of level ectopic CD4 expression, which cannot be trapped by MACS, causes an immunogenic reaction in the host heart after transplantation. We did not assess the immunogenic reaction or local inflammation of the transplanted mice. Further study is needed to compare the miR-switch-MACS method and conventional antibody-based methods from an immunological perspective. However, this concern is mitigated by the rapid degradation of the transfected mRNA and the absent CD4 expression in the final product of purified iPSC-CMs (Figures 2D, 3E, and Table S1). Additionally, the miR-switch-MACS method purifies cells by negative selection, which needs no genetic modification of the cell (Figure 1C). Thus, this method is assumed to be safe for clinical applications.

We previously reported the miR-Bim switch as another option to bypass the flow cytometry sorting process, as this switch uses pro-apoptotic Bim to automatically eliminate non-target cells after the miR-switch induction (Miki et al., 2015). However, we found that this method was inferior to the miR-switch-MACS method in terms of iPSC-CM purification efficiency (Figure S5 and Table S6). The reason might be that more steps are needed for the Bim-induced apoptosis, whereas the MACS-based selection simply depends on CD4 expression.

Figure 6. Flow cytometric, immunostaining and qPCR analysis of cells in subtype-specific iPSC-CMs

(A) Immunostaining of cells differentiated using the standard protocol and purified using miR-208a-switch.

(B and E) Flow cytometric analysis of cells differentiated using the atrial (B) and nodal (E) protocols. (Left) The percentage of troponin T-positive cells and cells that reacted to miR-208a switch before purification. (right) Troponin T-positive cells were significantly increased (B, 95.4 ± 3.3%; and E, 95.2 ± 2.4%) after the final purification. The values were acquired from three biologically independent measurements.

(C and F) qPCR analysis of ventricular-related (MYL2 and IRX4), atrial-related genes (COUPTF-II and MYL7) (C) and nodal-related genes (SHOX2 and ISL1) (F) in cells before purification, after purification with the conventional antibody-based method, and after purification with the miR-208a-switch. The values were acquired from three biologically independent measurements.

(D and G) Immunostaining of purified iPSC-CMs using miR-208a switch with the atrial (D) and nodal protocols (G). All scale bars, 100 μm. The values are denoted as means. All error bars represent the standard deviation. *p < 0.05, **p < 0.01, ***p < 0.001, and ****p < 0.0001, by a paired t-test.

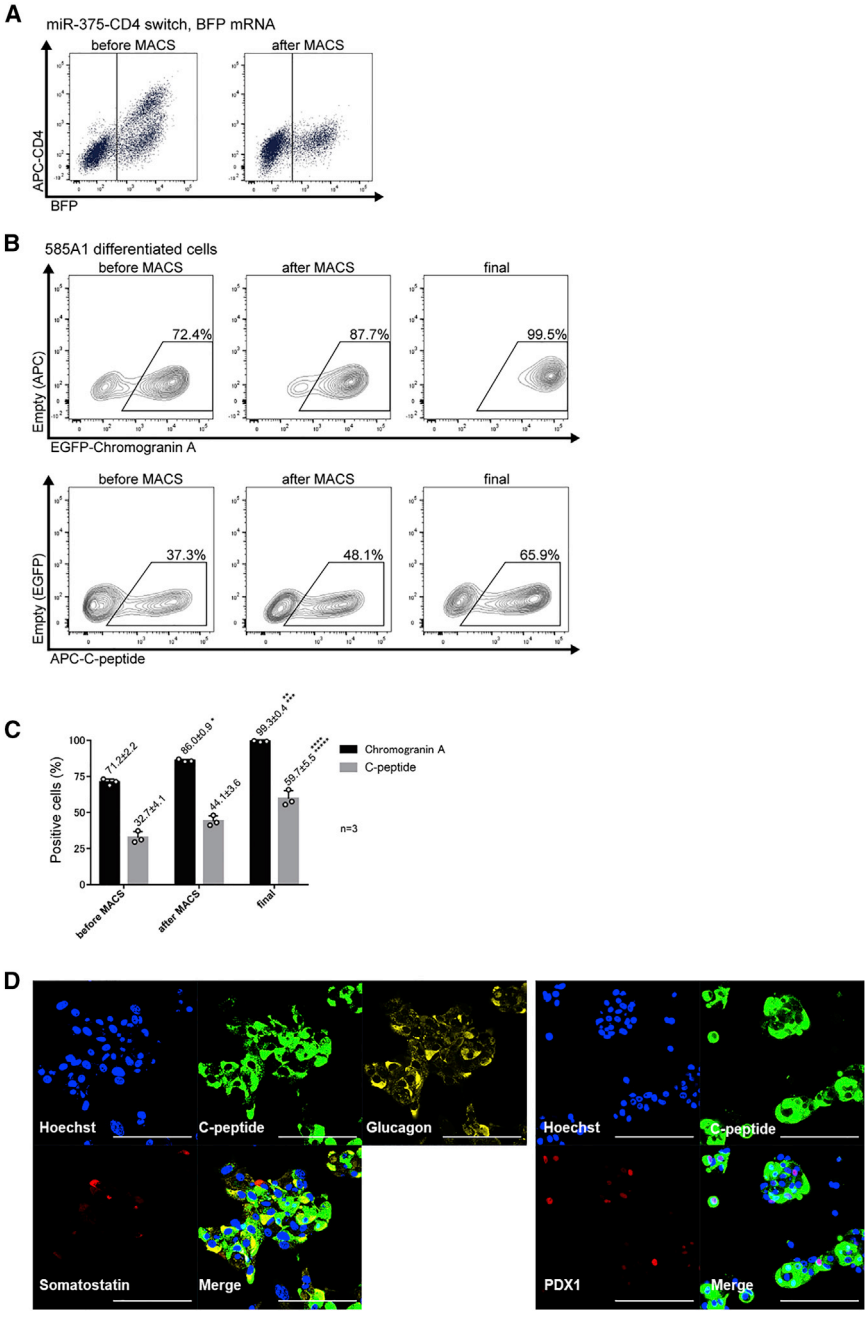

Figure 7. Purification of pancreatic cells using miR-375-CD4 switch and MACS

(A) The transfection of 300 ng miR-375-CD4-switch to differentiated 585A1 iPSCs. Representative data from three biologically independent experiments are shown. After MACS sorting, CD4-positive cells were eliminated.

(B) Representative data of chromogranin A- and C-peptide positive differentiated 585A1 iPSCs before MACS, after MACS, and after purification with puromycin (final) (n = 3). Representative data from three biologically independent experiments are shown. The boxed areas indicate chromogranin A-positive cells (upper panels) and C-peptide-positive cells (lower panels).

(C) The percentage of chromogranin A- and C-peptide positive differentiated 585A1 iPSCs before MACS, after MACS, and after purification. Data were collected from three biologically independent experiments. The values are denoted as mean ± standard deviation. *p < 0.001 versus the corresponding sample before MACS, **p < 0.001 versus the corresponding sample after MACS, ***p < 0.001 versus the corresponding sample before MACS, ****p < 0.015 versus the corresponding sample after MACS, *****p < 0.005 versus the corresponding sample before MACS. These were analyzed by the Bonferroni-Dunn test. The actual values are shown in Table S7.

(D) Immunostaining of the purified insulin-producing cells using the miR-375 switch-MACS method. Scale bars, 100 μm.

We also demonstrated that the miR-switch-MACS method can purify another cell type: insulin-producing cells. Notably, few methods have reported the efficient purification of this cell type with specific antibodies. The combination of miR-375-CD4 switch and -MACS showed more than 99% purification of chromogranin A-positive cells and approximately 60% of C-peptide-positive cells after eliminating untransfected cells by puromycin selection (Figures 7B, 7C, and Table S7). MiR-375 is one of the most abundant miRNAs in insulin-secreting β cells; however, it is also expressed in immature pancreatic endocrine precursor cells (Eliasson, 2017). Chromogranin A is also expressed widely in immature pancreatic endocrine precursor cells, which have polyhormonal aspects (Karlsson, 2001; Rieck et al., 2012), as well as in mature endocrine cells. In addition, immunostaining showed that some purified cells expressed PDX1 (Figure 7D). PDX1 is expressed in functional β cells and essential for maintaining mature β cell function

(Ahlgren et al., 1998; Wang et al., 2001). Thus, these findings suggest that the miR-375-switch-MACS method could purify endocrine precursor cells at a high efficiency, and importantly the purified cells include insulin-producing β cells. Since some studies have reported pancreatic cells are mature in the kidney subcapsule of immunodeficient mice after transplantation, pancreatic endocrine precursor cells purified by the miR-375-switch-MACS method may be a potential candidate for regenerative cell therapy for patients with diabetes (Toyoda et al., 2015). To isolate more mature C-peptide-positive insulin-producing cells, an miR-switch that senses miRNAs specifically expressed in mature insulin-producing cells is desired.

In the present study, we demonstrate that the miR-switch-MACS method is applicable to two types of cells (CMs and insulin-producing cells). However, miR-switch technology may be limited to cell types that uniquely have a miRNA specifically present or absent in such cell types. One solution to this problem is to use multiple miR-switches (Endo et al., 2016, 2019; Fujita et al., 2022) or miR-switch-based logic circuits, such as AND, OR, NAND, NOR, and XOR gates (Matsuura et al., 2018). Such multiple miR-switches and circuits may assist in purifying complicated cell populations. As for the purification of iPSC-CMs, cultivation under a glucose-depleted and lactate-abundant condition is also an option (Burridge et al., 2014; Tohyama et al., 2013). This type of metabolic selection may also be applicable to other types of cells. It is important to use a proper purification method for each type of cell.

For large-scale purification by the miR-switch-MACS method, the efficient delivery of synthetic RNAs into large amounts of cells must be addressed. We thus optimized the lipofection method and eventually achieved more than 70% transfection efficiency (Figures 2E, S2, and Table S2). The development of a cost-efficient transfection method with higher introduction efficiency (near 100%) would benefit the clinical application of this RNA-based technology. Additionally, puromycin selection after transfecting puromycin-resistant gene-coding mRNA can eliminate untransfected cell population before transplantation. Although RNA transfection could affect some cells, our transcriptome analysis showed only negligible differences in RNA expression profiles between ours and conventional purification methods (Figure 4). Moreover, iPSC-CMs purified by the miR-switch-MACS method were robustly engrafted *in vivo* and improved cardiac function according to acute myocardial infarction mouse models (Figures 5 and S4). These findings suggest the versatility of our method for regenerative cell transplantation therapies. Before future clinical application, however, larger animal models, such as pigs and monkeys, are needed.

In addition, the miR-switch-MACS method could be applied to atrial and nodal iPSC-CMs as well as ventricular ones. It has been reported that mimicking the developmental signal pathway by decreasing the concentration of BMP4 and activin A and adding retinoic acid or inhibiting fibroblast growth factor signaling can generate atrial or nodal CMs from iPSCs (Lee et al., 2017; Protze et al., 2017). Our subtype-specific protocols successfully differentiated atrial and nodal iPSC-CMs, and miR-208a switch could purify them. Disease modeling and future clinical application of atrial and nodal iPSC-CMs, such as atrial fibrillation and biological pacemakers, ideally require a pure CM population. However, miR-208a switch could not purify each subtype from one another. Future work should aim to produce subtype-specific miR-switches.

In conclusion, we developed a novel method for large-scale cell purification that combines miR-switch-MACS technologies. We designed a miR-switch that encodes the CD4 cell surface protein tagged with complementary sequences against the targeted miRNA. Using CD4 microbeads and MACS, we could easily and efficiently purify iPSC-CMs of several subtypes and insulin-producing cells at large scale. We also demonstrated that human iPSC-CMs purified by this method could be engrafted in a mouse model of acute myocardial infarction.

EXPERIMENTAL PROCEDURES

Human iPSC lines, cell culture and cardiac differentiation

Experiments with human iPSCs were approved by the ethics committee of the Department of Medicine and Graduate School of Medicine, Kyoto University. We used three human iPSC lines (201B7, 409B2, and 692D2), a fourth line into which a human MYH6 promoter driven-EGFP reporter cassette was integrated (201B7-MYH6-EGFP) (Funakoshi et al., 2016; Ohnuki et al., 2009), and a fifth line into which a CAG promoter-driven luciferase-expressing cassette was integrated (201B7-luc) (Funakoshi et al., 2016).

Human iPSCs were maintained as previously reported (Hatani et al., 2018b). Briefly, iPSCs were maintained on SNL feeders in primate ES cell medium (ReproCELL, cat. no. RCHEMD001) supplemented with 4 ng/mL recombinant human basic FGF (rhbFGF) (Wako, cat. no. 060–04543).

iPSCs were induced to differentiate into CMs using a modified embryoid body method as previously described (Funakoshi et al., 2016; Hatani et al., 2018b; Yang et al., 2008). Briefly, on day 0, iPSCs were dissociated, and EBs were generated in 10-cm low-attachment plates (Corning, cat. no. 3262) with StemPro-34 media (Life Technologies, cat. no. 10639-011) in the presence of 2 mM L-glutamine (Life Technologies), 4×10^{-4} M monothioglycerol (MTG; Sigma-Aldrich), 50 μg/mL ascorbic acid (AA; Sigma-Aldrich), 150 μg/mL transferrin (Roche), 10 μM Y-27632 (Wako, cat. no. 253–00513), and 2 ng/mL rhBMP4 (R&D Systems, cat.

no. 314-BP). After 24 h, the EBs were cultured in StemPro-34 media containing 2 mM L-glutamine, 4×10^{-4} M MTG, 50 μg/mL AA, 150 μg/mL transferrin, 10 ng/mL rhBMP4, 5 ng/mL rhbFGF (R&D Systems, cat. no. 233-FB), and 6 ng/mL rh activin A (R&D Systems, cat. no. 338-AC) for ventricular differentiation. In the protocol for atrial differentiation, rhBNP4 and rh activin A were 3 ng/mL and 4 ng/mL, respectively. In the protocol for nodal differentiation, rhBNP4 and rh activin A were 3 ng/mL and 1 ng/mL, respectively. On day 4, the EBs were suspended in StemPro-34 media supplemented with 2 mM L-glutamine, 4×10^{-4} M MTG, 50 μg/mL AA, 150 μg/mL transferrin, 10 ng/mL rhVEGF (R&D Systems, cat. no. 293-VE), and 1 μM Wnt inhibitor IWP-3 (Stemgent, cat. no. 04–0035) for 3 days. For the atrial protocol, 2 μM all-trans-retinoic acid (RA; Wako, cat. no. 182–01116) were added. For the nodal protocol, 2 μM RA, 0.25 ng/mL rhBNP4, 5.4 μM SB431542 (Sigma-Aldrich, cat. no. S4317-5MG), and 200 nM FGFR inhibitor PD 173074 (Chemscene, cat. no. CS-0182) were added. On day 7, the media were changed to StemPro-34 media supplemented with 2 mM L-glutamine, 4×10^{-4} M MTG, 50 μg/mL AA, 150 μg/mL transferrin, 5 ng/mL rhbFGF, and 10 ng/mL rhVEGF. Cultures were maintained in these media with media change every 2–3 days.

Template DNA for *in vitro* transcription of mRNAs and miR-switches

Template DNAs were prepared as previously described (Miki et al., 2015). Briefly, each sequence encoding the protein was duplicated from each vector (Table S8). 5′untranslated region (UTR) and -3′UTR were also amplified by PCR. For the template DNAs of the mRNAs, 5′UTR, which does not encode miRNA target sequences, the protein encoding region, and 3′UTR were integrated and amplified by PCR with the T7FwdG3C primer and the Rev120A primer. For the template DNAs of the miR-switches, 5′UTRtemp_Txxx, the protein encoding region, and 3′UTR were integrated and amplified by PCR with the T7FwdB primer and the Rev120A primer. KOD-Plus-Neo (Toyobo, cat. no. KOD-401) was used as DNA polymerase.

The PCR products amplified from the plasmids were treated with *Dpn*I restriction enzyme (Toyobo, cat. no. DPN-101) for 30 min at 37 °C. The PCR products were purified using a MinElute PCR Purification Kit (QIAGEN, cat. no. 28006) according to the manufacturer's instructions. Complete sequences of the template DNAs for the mRNAs and miR-switches used are listed in Table S8.

Synthesis and purification of mRNAs and miR-switches

mRNAs and miR-switches were synthesized as previously described (Miki et al., 2015; Warren et al., 2010). Briefly, they were generated with a MEGAscript T7 Transcription Kit (Ambion, cat. no. AMB13345) and a modified protocol. Template DNAs, T7 enzyme, ATP, guanosine triphosphate, pseudo-UTP (Tri-Link Bio Technologies, cat. no. N-1019-10), 5-methyl-CTP (Tri-Link Bio Technologies, cat. no. N-1014-10) and Anti Reverse Cap Analog (Tri-Link Bio Technologies, cat. no. N-7003-10) were reacted at 37 °C for 4 h. Adding TURBO DNase, the reacted products were further incubated at 37 °C for 30 min. The resulting mRNAs and miR-switches were incubated with Antarctic Phosphatase (New England Biolabs, cat. no. M0289S) at 37 °C for 30 min. The RNeasy MinElute Cleanup Kit (QIAGEN, cat. no. 74204) was used to purify the mRNAs and miR-switches.

Transfection of mRNAs and miR-switches, MACS, and puromycin selection

mRNAs and miR-switches were transfected into day 15 iPSC-differentiated cells using Lipofectamine MessengerMAX Transfection Reagent (Invitrogen, cat. no. LMRNA008) according to the manufacturer's protocol with modification. The amount of mRNA or miR-switch was 300 ng, the transfected cell number was 1×10^6 according to a TC20-automated cell counter (Bio-Rad), and the volume of Lipofectamine MessengerMAX Transfection Reagent was 7.5 μL. After 24 h from the transfection of the mRNAs and miR-switches, MACS was done according to the manufacturer's protocol. MACSelect 4 MicroBeads (Miltenyi Biotec, cat. no. 130-070-101; 1:7.5), which are magnetic microbeads conjugated to monoclonal anti-human CD4 antibodies, were used. MidiMACS Separator (Miltenyi Biotec, cat. no. 130-042-302) was used to collect non-magnetic cells by trapping magnetically labeled cells on LD Columns (Miltenyi Biotec, cat. no. 130-042-901). In the experiments with a large number of cells, the amount of mRNAs, miR-switches and Lipofectamine MessengerMAX Transfection Reagent were increased in proportion to the number of applied cells, and the columns and separator described above were used for MACS. (According to the manufacturer's protocol, the maximum number of applied cells before MACS is 5×10^8 and the maximum number of purified cells after MACS is 1×10^8, per column.) After MACS purification, 2 μg/mL puromycin was administered for 48 h to exclude untransfected cells.

RNA sequencing and analysis

For the RNA expression analysis, we used 201B7 iPSCs and 201B7 iPSC-CMs purified by antibodies (CD172a/b positive, CD31 negative, CD49a negative, CD90 negative, and CD140b negative) (Dubois et al., 2011) or purified by a miR-208a-CD4 switch and MACS. The cells were lysed with QIAzol Lysis Reagent (QIAGEN, cat. no. 79306), and total RNA was extracted using a RNeasy Mini Kit (QIAGEN, cat. no. 74104). The library construction and sequencing were performed using the TruSeq Stranded Total RNA Library Prep Kit with Ribo-Zero Gold Set A (48 samples) and Set B (48 samples) (Illumina, cat. no. RS-122-2301 and RS-122-2302) and NextSeq 500/550 High Output Kit v2 (75 cycles) (Illumina, cat. no. TG-160-2005). The quality of raw single-end reads were evaluated using RSeQC (ver. 2.6.4) (Wang et al., 2012). Before mapping, raw reads were trimmed with cutadapt (ver. 1.14) (Martin, 2011), and the removed reads were mapped in human rRNA and tRNA by bowtie2 (ver. 2.2.5) (Langmead and Salzberg, 2012). Trimmed reads were mapped to the human genome (GRCh38) using STAR (ver. 2.5.3a) (Dobin et al., 2013). Aligned reads were assigned using HTSeq (ver. 0.9.1) with GENCODE annotation (ver. 27) (Anders et al., 2015). In R (ver. 3.4.3), the counts were normalized by DESeq2 (ver. 1.18.1) (Love et al., 2014), and a heatmap with clustering was produced by pheatmap (ver. 1.0.12).

Data and code availability

The RNA sequence data are available at the Gene Expression Omnibus (http://www.ncbi.nlm.nih.gov/geo/) under accession no. GSE153714.

SUPPLEMENTAL INFORMATION

Supplemental information can be found online at https://doi.org/10.1016/j.stemcr.2022.05.003.

AUTHOR CONTRIBUTIONS

Y.T. and T.H. equally contributed to this work as co-first authors. Y.T., T.H., K.C., T.T., K.O., T.K., H.S., and Y.Y. contributed to the design of the study. Y.T., T.H., and C.O. carried out the experiments. R.I. and A.K. performed the pancreatic differentiation. Y.T., T.H., M.N., and C.O. extracted and processed the RNA and analyzed the RNA data. Y.T., T.H., H.S., and Y.Y. wrote the manuscript.

ACKNOWLEDGMENTS

We greatly appreciate colleagues at our laboratories and the Department of Cardiovascular Medicine, Kyoto University, for their critical comments. We thank Peter Karagiannis for critical reading of the manuscript, and Misato Nishikawa and Azusa Inagaki for technical support. We would like to express our heartfelt gratitude to Yoko Uematsu and Kaoru Shimizu for their administrative support. Funding was provided by The Leducq Foundation (18CVD05) (Y.Y.), the Japan Society for the Promotion of Science (JSPS) KAKENHI No. 15H05722 (H.S.), No. 20H05626 (H.S.), No. 17H04176 (Y.Y.), and No. 21H02912 (Y.Y.), Research Center Network for Realization of Regenerative Medicine, Japan Agency of Medical Research and Development (AMED) (JP19bm0104001, JP19bm0204003, JP19bm0804008, and JP20bm0804022) (Y.Y., H.S.), the Research on Regulatory Science of Pharmaceuticals and Medical Devices, AMED (JP19mk0104117) (Y.Y.), the Research Project for Practical Applications of Regenerative Medicine, AMED (JP19bk0104095) (Y.Y.), the iPS Cell Research Fund (Y.Y., H.S., and T.H.) and the SECOM Science and Technology Foundation (Y.Y.).

CONFLICTS OF INTEREST

Y.Y. receives grants from Takeda Pharmaceutical Company. H.S. and Y.Y are the investigators of a record listed on the patent application (PCT/JP2016/062710 filed by Kyoto University on 22/04/2016, and PCT/JP2015/058466 filed by Kyoto University on 20/03/2015) related to this work. Y.Y. and S.F. are scientific advisors for Orizuru Therapeutics. H.S. owns shares and has an outside director of aceRNA Technologies Ltd.

Received: May 21, 2021
Revised: May 12, 2022
Accepted: May 13, 2022
Published: June 9, 2022

REFERENCES

Ahlgren, U., Jonsson, J., Jonsson, L., Simu, K., and Edlund, H. (1998). β-Cell-specific inactivation of the mouse*Ipf1/Pdx1* gene results in loss of the β-cell phenotype and maturity onset diabetes. Genes Dev. *12*, 1763–1768. https://doi.org/10.1101/gad.12.12.1763.

Ambros, V. (2001). microRNAs: tiny regulators with great potential. Cell *107*, 823–826. https://doi.org/10.1016/s0092-8674(01)00616-x.

Anders, S., Pyl, P.T., and Huber, W. (2015). HTSeq–a Python framework to work with high-throughput sequencing data. Bioinformatics *31*, 166–169. https://doi.org/10.1093/bioinformatics/btu638.

Bartel, D.P. (2004). MicroRNAs: genomics, biogenesis, mechanism, and function. Cell *116*, 281–297. https://doi.org/10.1016/s0092-8674(04)00045-5.

Burridge, P.W., Matsa, E., Shukla, P., Lin, Z.C., Churko, J.M., Ebert, A.D., Lan, F., Diecke, S., Huber, B., Mordwinkin, N.M., et al. (2014). Chemically defined generation of human cardiomyocytes. Nat. Methods *11*, 855–860. https://doi.org/10.1038/nmeth.2999.

Chong, J.J.H., Yang, X., Don, C.W., Minami, E., Liu, Y.W., Weyers, J.J., Mahoney, W.M., Van Biber, B., Cook, S.M., Palpant, N.J., et al. (2014). Human embryonic-stem-cell-derived cardiomyocytes regenerate non-human primate hearts. Nature *510*, 273–277. https://doi.org/10.1038/nature13233.

Dobin, A., Davis, C.A., Schlesinger, F., Drenkow, J., Zaleski, C., Jha, S., Batut, P., Chaisson, M., and Gingeras, T.R. (2013). STAR: ultrafast universal RNA-seq aligner. Bioinformatics *29*, 15–21. https://doi.org/10.1093/bioinformatics/bts635.

Dubois, N.C., Craft, A.M., Sharma, P., Elliott, D.A., Stanley, E.G., Elefanty, A.G., Gramolini, A., and Keller, G. (2011). SIRPA is a specific cell-surface marker for isolating cardiomyocytes derived from human pluripotent stem cells. Nat. Biotechnol. *29*, 1011–1018. https://doi.org/10.1038/nbt.2005.

Dunn, T.B., Noreen, H., Gillingham, K., Maurer, D., Ozturk, O.G., Pruett, T.L., Bray, R.A., Gebel, H.M., and Matas, A.J. (2011). Revisiting traditional risk factors for rejection and graft loss after kidney transplantation. Am. J. Transplant. *11*, 2132–2143. https://doi.org/10.1111/j.1600-6143.2011.03640.x.

Eliasson, L. (2017). The small RNA miR-375 - a pancreatic islet abundant miRNA with multiple roles in endocrine beta cell function. Mol. Cell. Endocrinol. *456*, 95–101. https://doi.org/10.1016/j.mce.2017.02.043.

Endo, K., Hayashi, K., and Saito, H. (2016). High-resolution identification and separation of living cell types by multiple microRNA-responsive synthetic mRNAs. Sci. Rep. *6*, 21991. https://doi.org/10.1038/srep21991.

Endo, K., Hayashi, K., and Saito, H. (2019). Numerical operations in living cells by programmable RNA devices. Sci. Adv. *5*, eaax0835. https://doi.org/10.1126/sciadv.aax0835.

Fujita, Y., Hirosawa, M., Hayashi, K., Hatani, T., Yoshida, Y., Yamamoto, T., and Saito, H. (2022). A versatile and robust cell purification system with an RNA-only circuit composed of microRNA-responsive ON and OFF switches. Sci. Adv. *8*, eabj1793. https://doi.org/10.1126/sciadv.abj1793.

Funakoshi, S., Miki, K., Takaki, T., Okubo, C., Hatani, T., Chonabayashi, K., Nishikawa, M., Takei, I., Oishi, A., Narita, M., et al. (2016). Enhanced engraftment, proliferation, and therapeutic potential in heart using optimized human iPSC-derived cardiomyocytes. Sci. Rep. *6*, 19111. https://doi.org/10.1038/srep19111.

Hatani, T., Funakoshi, S., Deerinck, T.J., Bushong, E.A., Kimura, T., Takeshima, H., Ellisman, M.H., Hoshijima, M., and Yoshida, Y.

(2018a). Nano-structural analysis of engrafted human induced pluripotent stem cell-derived cardiomyocytes in mouse hearts using a genetic-probe APEX2. Biochem. Biophys. Res. Commun. *505*, 1251–1256. https://doi.org/10.1016/j.bbrc.2018.10.020.

Hatani, T., Miki, K., and Yoshida, Y. (2018b). Induction of human induced pluripotent stem cells to cardiomyocytes using embryoid bodies. Methods Mol. Biol. *1816*, 79–92. https://doi.org/10.1007/978-1-4939-8597-5_6.

Hattori, F., and Fukuda, K. (2012). Strategies for replacing myocytes with induced pluripotent stem in clinical protocols. Transplant. Rev. *26*, 223–232. https://doi.org/10.1016/j.trre.2011.09.003.

Karlsson, E. (2001). The role of pancreatic chromogranins in islet physiology. Curr. Mol. Med. *1*, 727–732. https://doi.org/10.2174/1566524013363294.

Langmead, B., and Salzberg, S.L. (2012). Fast gapped-read alignment with Bowtie 2. Nat. Methods *9*, 357–359. https://doi.org/10.1038/nmeth.1923.

Lee, J.H., Protze, S.I., Laksman, Z., Backx, P.H., and Keller, G.M. (2017). Human pluripotent stem cell-derived atrial and ventricular cardiomyocytes develop from distinct mesoderm populations. Cell Stem Cell *21*, 179–194.e4. https://doi.org/10.1016/j.stem.2017.07.003.

Love, M.I., Huber, W., and Anders, S. (2014). Moderated estimation of fold change and dispersion for RNA-seq data with DESeq2. Genome Biol. *15*, 550. https://doi.org/10.1186/s13059-014-0550-8.

Martin, M. (2011). Cutadapt removes adapter sequences from high-throughput sequencing reads. EMBnet *17*, 10. https://doi.org/10.14806/ej.17.1.200.

Matsuura, S., Ono, H., Kawasaki, S., Kuang, Y., Fujita, Y., and Saito, H. (2018). Synthetic RNA-based logic computation in mammalian cells. Nat. Commun. *9*, 4847. https://doi.org/10.1038/s41467-018-07181-2.

Miki, K., Endo, K., Takahashi, S., Funakoshi, S., Takei, I., Katayama, S., Toyoda, T., Kotaka, M., Takaki, T., Umeda, M., et al. (2015). Efficient detection and purification of cell populations using synthetic MicroRNA switches. Cell Stem Cell *16*, 699–711. https://doi.org/10.1016/j.stem.2015.04.005.

Nakanishi, H., and Saito, H. (2019). Mammalian gene circuits with biomolecule-responsive RNA devices. Curr. Opin. Chem. Biol. *52*, 16–22. https://doi.org/10.1016/j.cbpa.2019.04.013.

Ohno, H., Akamine, S., and Saito, H. (2020). Synthetic mRNA-based Systems in mammalian cells. Adv Biosyst. *4*, e1900247. https://doi.org/10.1002/adbi.201900247.

Ohnuki, M., Takahashi, K., and Yamanaka, S. (2009). Generation and characterization of human induced pluripotent stem cells. Current Protoc. Stem Cell Biol. *Chapter 4*. Unit 4A 2. https://doi.org/10.1002/9780470151808.sc04a02s9.

Osborn, L., Hession, C., Tizard, R., Vassallo, C., Luhowskyj, S., Chi-Rosso, G., and Lobb, R. (1989). Direct expression cloning of vascular cell adhesion molecule 1, a cytokine-induced endothelial protein that binds to lymphocytes. Cell *59*, 1203–1211. https://doi.org/10.1016/0092-8674(89)90775-7.

Protze, S.I., Liu, J., Nussinovitch, U., Ohana, L., Backx, P.H., Gepstein, L., and Keller, G.M. (2017). Sinoatrial node cardiomyocytes derived from human pluripotent cells function as a biological pacemaker. Nat. Biotechnol. *35*, 56–68. https://doi.org/10.1038/nbt.3745.

Rieck, S., Bankaitis, E.D., and Wright, C.V. (2012). Lineage determinants in early endocrine development. Semin. Cell Dev. Biol. *23*, 673–684. https://doi.org/10.1016/j.semcdb.2012.06.005.

Sanganalmath, S.K., and Bolli, R. (2013). Cell therapy for heart failure: a comprehensive overview of experimental and clinical studies, current challenges, and future directions. Circ. Res. *113*, 810–834. https://doi.org/10.1161/circresaha.113.300219.

Shiba, Y., Gomibuchi, T., Seto, T., Wada, Y., Ichimura, H., Tanaka, Y., Ogasawara, T., Okada, K., Shiba, N., Sakamoto, K., et al. (2016). Allogeneic transplantation of iPS cell-derived cardiomyocytes regenerates primate hearts. Nature *538*, 388–391. https://doi.org/10.1038/nature19815.

Tohyama, S., Hattori, F., Sano, M., Hishiki, T., Nagahata, Y., Matsuura, T., Hashimoto, H., Suzuki, T., Yamashita, H., Satoh, Y., et al. (2013). Distinct metabolic flow enables large-scale purification of mouse and human pluripotent stem cell-derived cardiomyocytes. Cell Stem Cell *12*, 127–137. https://doi.org/10.1016/j.stem.2012.09.013.

Toyoda, T., Mae, S.I., Tanaka, H., Kondo, Y., Funato, M., Hosokawa, Y., Sudo, T., Kawaguchi, Y., and Osafune, K. (2015). Cell aggregation optimizes the differentiation of human ESCs and iPSCs into pancreatic bud-like progenitor cells. Stem Cell Res. *14*, 185–197. https://doi.org/10.1016/j.scr.2015.01.007.

Virani, S.S., Alonso, A., Benjamin, E.J., Bittencourt, M.S., Callaway, C.W., Carson, A.P., Chamberlain, A.M., Chang, A.R., Cheng, S., Delling, F.N., et al. (2020). Heart disease and stroke statistics-2020 update: a report from the American heart association. Circulation *141*, e139–e596. https://doi.org/10.1161/cir.0000000000000757.

Wang, H., Maechler, P., Ritz-Laser, B., Hagenfeldt, K.A., Ishihara, H., Philippe, J., and Wollheim, C.B. (2001). Pdx1 level defines pancreatic gene expression pattern and cell lineage differentiation. J. Biol. Chem. *276*, 25279–25286. https://doi.org/10.1074/jbc.M101233200.

Wang, L., Wang, S., and Li, W. (2012). RSeQC: quality control of RNA-seq experiments. Bioinformatics *28*, 2184–2185. https://doi.org/10.1093/bioinformatics/bts356.

Warren, L., Manos, P.D., Ahfeldt, T., Loh, Y.H., Li, H., Lau, F., Ebina, W., Mandal, P.K., Smith, Z.D., Meissner, A., et al. (2010). Highly efficient reprogramming to pluripotency and directed differentiation of human cells with synthetic modified mRNA. Cell Stem Cell *7*, 618–630. https://doi.org/10.1016/j.stem.2010.08.012.

Yang, L., Soonpaa, M.H., Adler, E.D., Roepke, T.K., Kattman, S.J., Kennedy, M., Henckaerts, E., Bonham, K., Abbott, G.W., Linden, R.M., et al. (2008). Human cardiovascular progenitor cells develop from a KDR+ embryonic-stem-cell-derived population. Nature *453*, 524–528. https://doi.org/10.1038/nature06894.

Stem Cell Reports, Volume *17*

Supplemental Information

Purification of human iPSC-derived cells at large scale using microRNA switch and magnetic-activated cell sorting

Yuta Tsujisaka, Takeshi Hatani, Chikako Okubo, Ryo Ito, Azuma Kimura, Megumi Narita, Kazuhisa Chonabayashi, Shunsuke Funakoshi, Antonio Lucena-Cacace, Taro Toyoda, Kenji Osafune, Takeshi Kimura, Hirohide Saito, and Yoshinori Yoshida

Figure S1

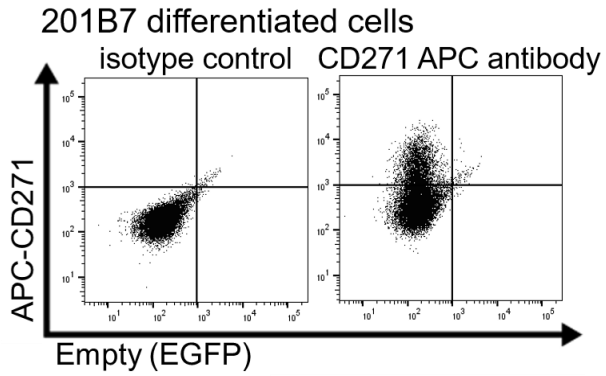

Figure S1. CD271 expression in cells differentiated from the 201B7 iPSC line (related to Figure 2)

Flow cytometric analysis showed that some differentiated cells expressed CD271.

Figure S2

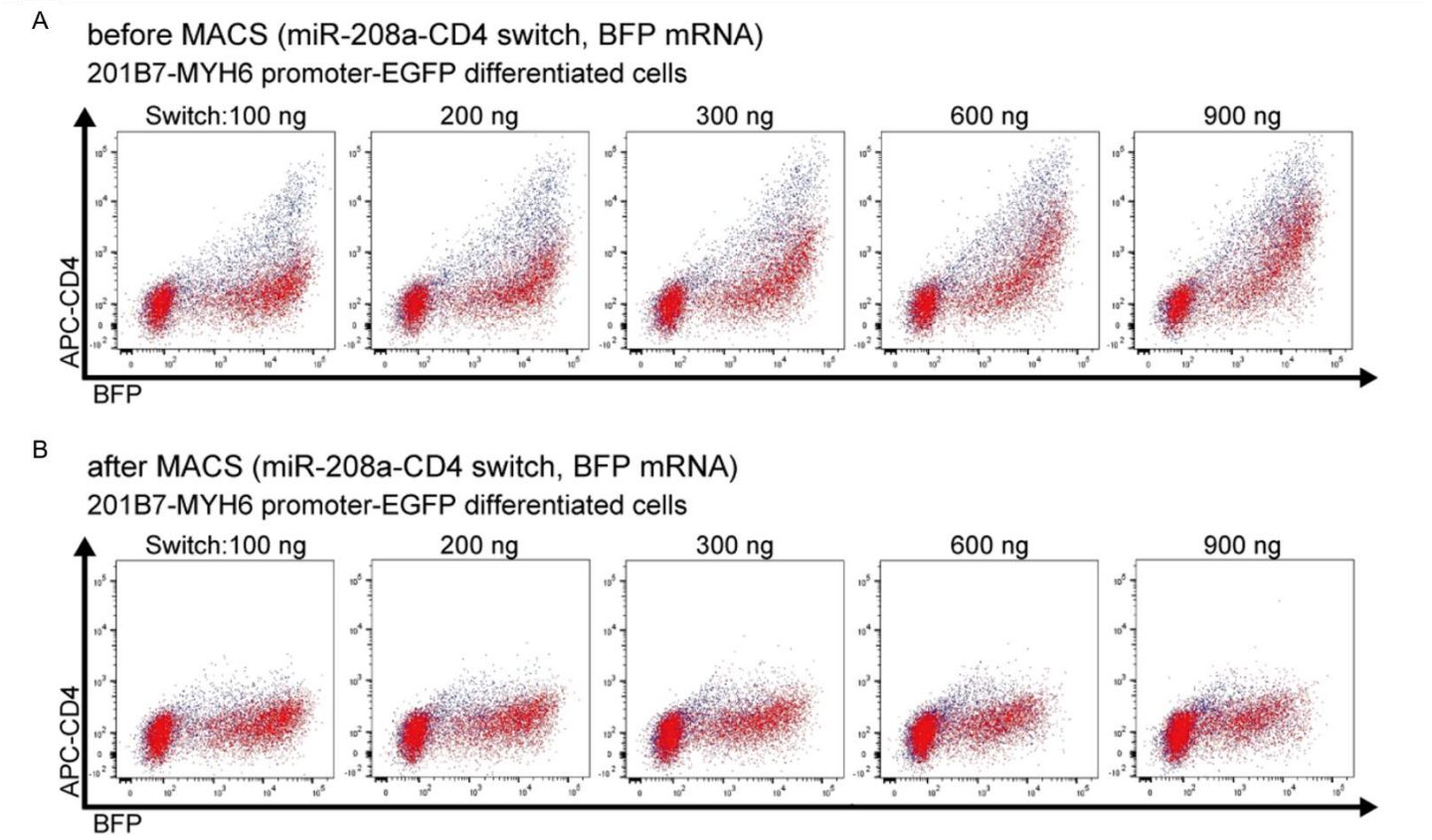

Figure S2. Purification efficiency of CMs depends on amount of miR-208a-CD4 switch (related to Figure 2)

The transfection of 100, 200, 300, 600 and 900 ng of miR-208a-CD4 switch and 300 ng of control BFP mRNA to 201B7-MYH6 promoter-EGFP differentiated cells. Red shows EGFP positive cells (CMs) and blue shows EGFP negative cells (non-CMs). Representative data from two biological independent experiments are shown. (A) Before MACS. As more miRNA switch was transfected, CMs and non-CMs expressed more CD4 on their surface. (B) After MACS. CD4 positive cells were clearly eliminated. Table S2 shows results related to Figure S2.

Figure S3

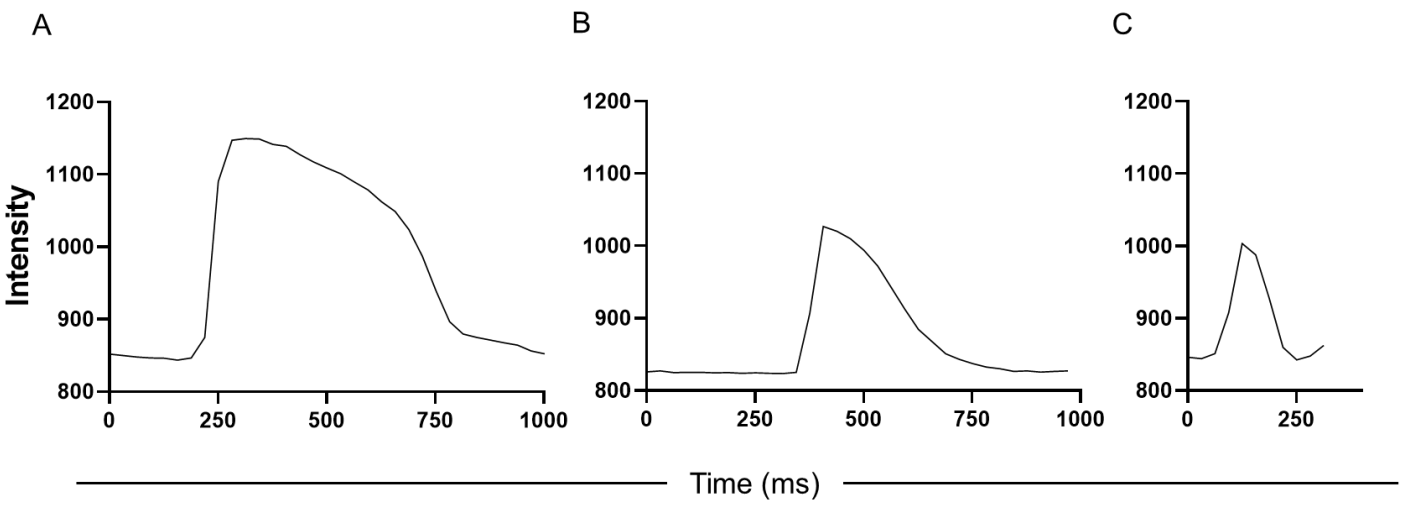

Figure S3. Representative action potentials of the final purified iPSC-CMs. (related to Figures 3 and 6)

The action potential duration (APD) is shown in Table S4. (A) A ventricular action potential with a long plateau phase was observed in the ventricular protocol. (B) An atrial action potential with an absent of a prominent plateau phase was observed in the atrial protocol. (C) A nodal action potential with slow action potential upstroke and phase four depolarization was observed in the nodal protocol.

Figure S4

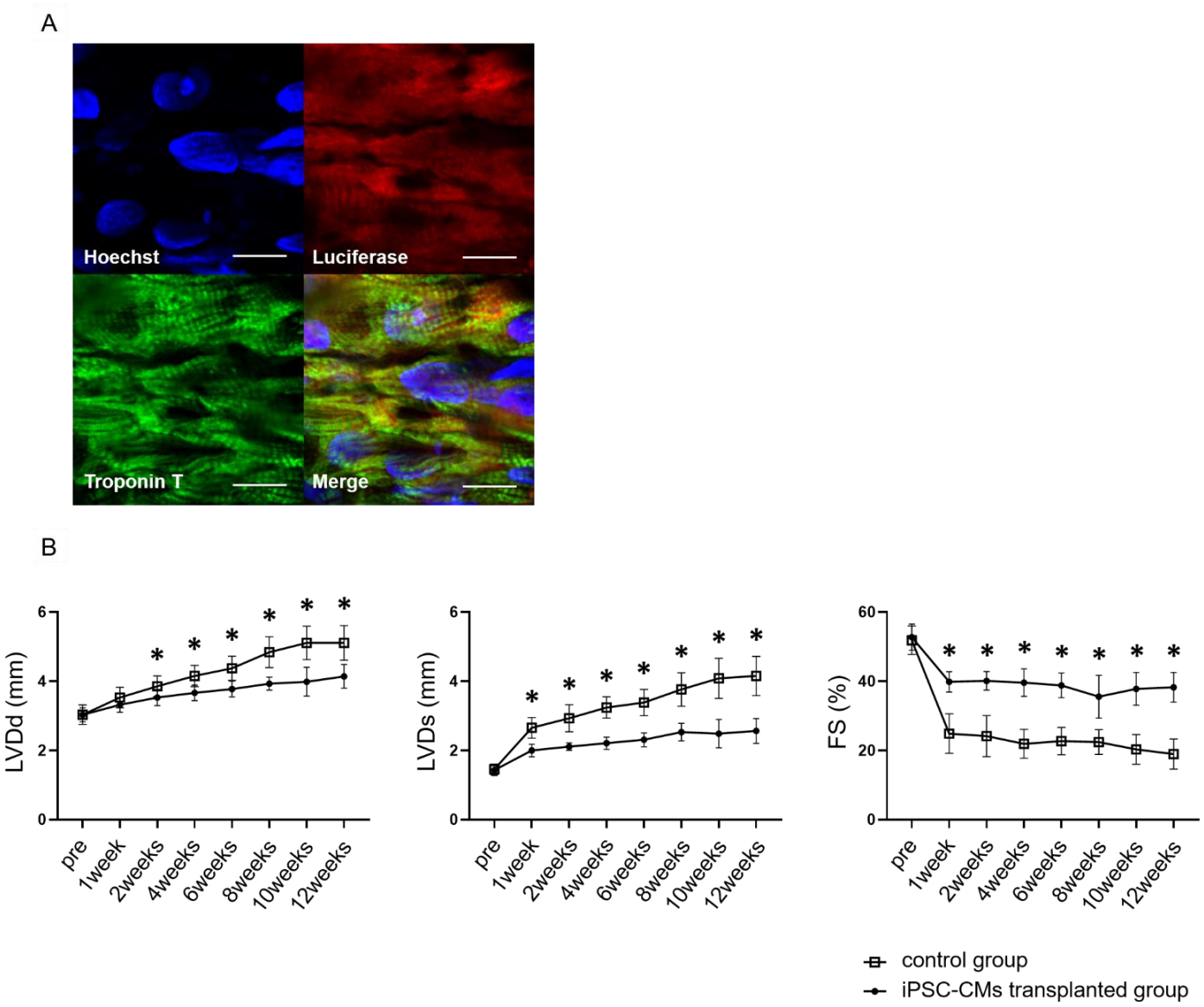

Figure S4. Immunostaining and echocardiographic data of mouse hearts transplanted with purified iPSC-CMs (related to Figure 5)

(A) Immunostaining of Troponin T (green) with high magnification showed that transplanted iPSC-CMs formed sarcomere structures. Scale bars: 10 μm. (B) The cardiac function of the iPSC-CM-transplanted group (n=9) and the control group (n=9) was assessed by echocardiography. LV dimensions (LVDd and LVDs) were increased, and the fractional shortening (FS) was decreased just after the myocardial infarction in both groups. However, compared with the control group, the

degree of changes were relatively small in the iPSC-CM-transplanted group. At one week after the injection, FS was significantly higher in the iPSC-CM-transplanted group compared with the control group. Similarly, LVDd at two weeks after the injection was significantly lower. These differences were maintained throughout the three-months follow-up period. The values are denoted as means. All error bars represent SD. *$P < 0.05$ by the unpaired t test.

Figure S5

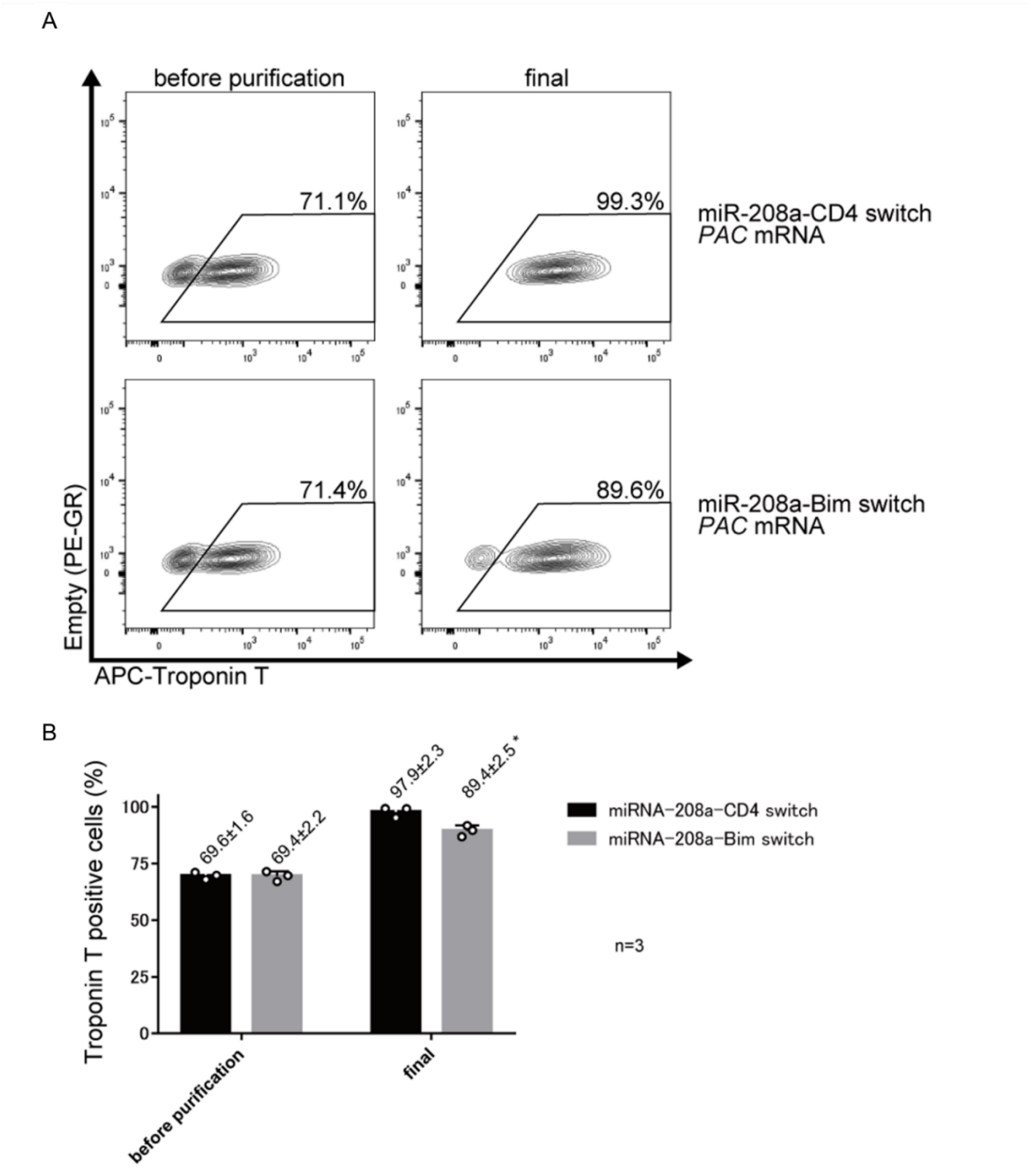

Figure S5. Comparison of miR-208a-CD4 switch and miR-208a-Bim switch (related to Figure 3)

(A) Troponin T positive differentiated 201B7 iPSCs before and after purification (final). Representative data from three biological independent experiments are shown. In the upper panels, 300 ng of miR-208a-CD4 switch and 300 ng of PAC

mRNA were transfected. In the lower panels, 300 ng of miR-208a-Bim switch and 300 ng of PAC mRNA were transfected. Troponin T positive cells are shown in red, and Troponin T negative cells are shown in blue. (B) Troponin T positive differentiated 201B7 iPSCs before purification and after purification. Data are from three biologically independent measurements. The values are denoted as means ± SD. A significant difference was observed in CM purity between the miR-208a-CD4 switch group and miR-208a-Bim switch group (* $P<0.001$, by a two-way ANOVA with repeated measures test). The actual values are shown in Table S6.

Table S1. Time course of mRNA expression (n=3) (related to Figure 2)

Time (days after transfection)		0.5	1	2	3	4	5	6	7	8	9
BFP positive cells (%)	1st	71.2	84.0	77.8	81.0	52.4	43.0	19.9	13.0	11.1	5.9
	2nd	68.4	73.6	81.2	69.6	60.6	32.8	26.6	20.4	17.8	2.8
	3rd	77.2	81.3	84.9	76.5	67.1	38.7	23.5	20.6	18.0	9.4
	mean	72.3	79.6	81.3	75.7	60.0	38.2	23.3	18.0	15.6	6.0
	SD	4.5	5.4	3.6	5.7	7.4	5.1	3.4	4.3	3.9	3.3

Table S2. Purification efficiency of CMs depends on the amount of miRNA switch (n=2) (related to Figure 2 and S2)

	Amount of miRNA switch (ng)	100	200	300	600	900
Before MACS	Transfection efficiency (%)	74.2 ± 1.5	74.3 ± 1.1	76.0 ± 0.4	75.8 ± 2.1	75.5 ± 1.3
	Percentage of CMs (%)	71.4 ± 1.6	71.5 ± 1.1	71.9 ± 1.1	71.2 ± 0.5	71.2 ± 1.8
	Estimated percentage of CMs retained after MACS (%)	68.8 ± 0.9	59.7 ± 1.1	53.2 ± 1.5	38.6 ± 1.5	21.1 ± 2.4
After MACS	The degree of CM purity among successfully transfected cells (%)	89.0 ± 0.2	91.7 ± 0.6	96.6 ± 0.3	97.6 ± 0.2	98.5 ± 0.4

Table S2. Purification efficiency of CMs depends on the amount of miRNA switch (n=2) (related to Figure 2 and S2)

100, 200, 300, 600 and 900 ng of miR-208a-CD4 switch were respectively transfected to 201B7-MYH6 promoter-EGFP differentiated cells with 300 ng of control BFP mRNA. The transfection efficiency is defined as BFP positive cells / all cells. The proportion of CMs is defined as EGFP positive cells / all cells. The estimated proportion of CMs retained after MACS compared with before MACS was calculated as (APC negative + EGFP positive cells) / EGFP positive cells before MACS. After MACS, the degree of CM purity among successfully transfected cells is defined as EGFP positive cells / BFP positive cells. The values are denoted as means ± SD. Data were from two biologically independent measurements.

Table S3. Troponin T positive cells during miR-208a-CD4 switch and MACS purification (n=3) (related to Figure 3)

Troponin T positive cells (%)		before MACS	after MACS	final
201B7	1st	68.8	82.1	98.9
	2nd	75.1	88.8	98.7
	3rd	63.9	82.7	96.1
	mean	69.3	84.5	97.9
	SD	5.6	3.7	1.6
409B2	1st	73.6	83.5	98.2
	2nd	76.5	85.2	98.7
	3rd	67.7	84.2	97.0
	mean	72.6	84.3	98.0
	SD	4.5	0.9	0.9
692D2	1st	70.2	85.1	97.8
	2nd	66.6	82.7	95.2
	3rd	75.6	86.4	98.1
	mean	70.8	84.7	97.0
	SD	4.5	1.9	1.6

Table S4. Electrophysiological characteristics of the final purified CMs (related to Figures 3 and 6)

	APD50 (ms)	APD90 (ms)	APD90 / APD50 (ms)
Ventricular iPSC-CMs	398 ± 6.1	493 ± 38	1.24 ± 0.08
Atrial iPSC-CMs	218 ± 34	385 ± 79	1.76 ± 0.13
Nodal iPSC-CMs	93 ± 1.6	151 ± 2.7	1.62 ± 0.02

Table S4. Electrophysiological characteristics of the final purified CMs (related to Figures 3 and 6)

Action potentials of the final purified iPSC-CMs were recorded using a voltage sensitive fluorescent probe. 10 beats per cells for 10 cells (10 ROIs; a total of 100 beats) were recorded. Action potential durations (APD) at 50% repolarization (APD50) and APD90 were measured, and the ratio of APD90/APD50 was calculated. APD90 / APD50 <1.4, APD90 / APD50 >1.7 and 1.4< APD90 / APD50 <1.7 characterizes ventricular, atrial and nodal action potentials, respectively. Representative recorded action potentials are shown in Figure S3. The values are denoted as means ± SD.

Table S5. Time required to get purified CMs (n=3) (related to Figure 3)

Method	Experiment	Applied cells	Troponin T positive rate before MACS or FACS (%)	Procedural time	Final purified cells	Troponin T positive rate of final purified cells(%)
MACS	1st	3.21×10^8	68.8	28min02sec	1.72×10^8	98.9
	2nd	3.01×10^8	75.1	26min30sec	1.82×10^8	98.7
	3rd	3.42×10^8	63.9	29min58sec	2.00×10^8	97.1
	mean	3.21×10^8	69.2	28min10sec	1.85×10^8	98.2
	SD	0.21×10^8	5.6	104sec	0.14×10^8	0.99
FACS Aria II	1st		68.8	24min56sec	1.12×10^6	98.4
	2nd		75.1	30min32sec	1.20×10^6	99.1
	3rd		63.9	26min08sec	1.14×10^6	97.8
	mean		69.2	27min12sec	1.15×10^6	98.4
	SD		5.6	177sec	0.042×10^6	0.65

Table S5. The required time to get purified CMs (n=3) (related to Figure 3)

In the miRNA-switch-MACS method, $3.21 \pm 0.21\times10^8$ differentiated cells were applied, resulting in $1.85 \pm 0.14\times10^8$ final purified cells after MACS and subsequent puromycin selection. The procedural time was defined as the time for MACS. On the other hand, $1.15 \pm 0.042\times10^6$ purified cells, which is less than 1% that with the miRNA-switch-MACS method, were obtained in FACS method. The procedural time, defined as the time for FACS, is similar to that of MACS. Troponin T positive rates of the final purified cells were similar between methods.

Table S6. Troponin T positive cells using miR-208a-CD4 switch and miR-208a-Bim-switch (n=3) (related to Figure S5)

Troponin T positive cells (%)	miRNA-208a CD4 switch		miRNA-208a Bim switch	
	before purification	final	before purification	final
1st	67.9	95.2	67.1	86.8
2nd	71.1	99.3	71.4	89.6
3rd	69.8	99.2	69.7	91.7
mean	69.6	97.9	69.4	89.4
SD	1.6	2.3	2.2	2.5

Table S7. Chromogranin A and C-peptide positive cells (n=3) (related to Figure 7)

	Chromogranin A positive cells (%)			C-peptide positive cells (%)		
	before MACS	after MACS	final	before MACS	after MACS	final
1st	68.9	87.0	99.7	31.2	43.1	57.7
2nd	73.2	85.4	98.9	29.6	41.2	55.5
3rd	71.4	85.7	99.3	37.3	48.1	65.9
mean	71.2	86.0	99.3	32.7	44.1	59.7
SD	2.2	0.9	0.4	4.1	3.6	5.5

Table S8. Sequences of primers, templates and template DNAs for mRNAs and miR-switches (in reference to STAR methods)

Supplemental experimental procedures

Human iPSC lines, cell culture and pancreatic differentiation

Human iPSC line 585A1 was maintained as previously reported (Hatani et al., 2018). Briefly, iPSCs were maintained by feeder-free cultures with Essential 8 medium (Life Technologies, cat. no. A1517001). iPSCs were induced to differentiate into pancreatic lineage as previously reported with modifications (Kimura et al., 2017; Toyoda et al., 2015). On day 0, iPSCs were dissociated and seeded on Matrigel (Becton Dickinson, cat. no. 354230)-coated plates with RPMI 1640 medium (NACALAI TESQUE, cat. no. 30264-56) in the presence of 2% (vol/vol) B27 supplement (B27, Thermo Fisher Scientific, cat. no. 17504044), 50 U/mL penicillin/streptomycin (P/S, Thermo Fisher Scientific, cat. no. 15140122), 100 ng/mL activin A (R&D Systems, cat. no. 338-AC), 3 μM CHIR99021 (Axon Medchem, cat. no. AXON1386) and 10 μM Y-27632 (Wako, cat. no. 251-00514). After 24 hours, the cells were cultured in RPMI 1640 medium containing 2% B27, 50 U/ml P/S, 100 ng/mL activin A and 1 μM CHIR99021. On day 3, the cells were cultured in RPMI 1640 medium containing 2% B27, 50 U/mL P/S and 100 ng/mL activin A. On day 4, the cells were cultured with Improved MEM Zinc Option (IMEM) medium (Thermo Fisher Scientific, cat. no. 10373017) supplemented with 1% B27, 100 U/mL P/S (IMEM-B27-P/S) and 50 ng/mL keratinocyte growth factor (KGF; R&D Systems, cat. no. 251-KG) for four days. On day 8, the cells were cultured in IMEM-B27-P/S containing 50 ng/mL KGF, 0.5 μM 3-Keto-N-aminoethyl-N'-aminocaproyldihydrocinnamoyl cyclopamine (KAAD-CYC, Toronto Research Chemicals, cat. no. K171000), 10 nM 4-[(E)-2-(5,6,7,8-Tetrahydro-5,5,8,8-tetramethyl-2-naphthalenyl)-1-propenyl] benzoic acid (TTNPB, Santa Cruz Biotechnology, cat. no. sc-203303) and 100 ng/mL NOGGIN (Pepro-tech, cat. no. 120-10C) for two days. On day 10, the cells were dissociated into single cells and seeded on Matrigel-coated plates with the same medium composition as day 8, except for the addition of 10 μM Y-27632. On day 11, the cells were cultured in IMEM-B27-P/S containing 100 ng/mL KGF, 50 ng/ml epidermal growth factor (EGF, R&D Systems, cat. no. 236-EG), 10 mM Nicotinamide (STEMCELL Technologies, cat. no. 07154) and 50 μM Y-27632 for four days. On day 15, the cells were dissociated into single cells and seeded on low-attachment plates (Greiner, cat. no. 651970) for aggregation cultures with the same medium composition as day 11, except for replacing 50 μM Y-27632 with 10 μM Y-27632. On day 17, the aggregates were cultured in IMEM-B27-P/S containing 1 μM RO4929097 (Selleck, cat. no. S1575), 10 μM Alk 5 inhibitor II (Wako, cat. no. 018-23023), 1 μM Triiodothyronine (Merck Millipore, cat. no. 64245) and 0.1 μM LDN193189 (Wako, cat. no. 124-06011) for four days. From days 21 to 28, the aggregates were cultured with the same medium composition as day 17, except for the removal of RO4929097.

Transplantation of human iPSC-CMs purified by miRNA switch and MACS

All experimental protocols involving animals were approved by the Kyoto University Animal Experimentation Committee, and procedures were performed in accordance with the Guidelines for Animal Experiments of Kyoto University and the Guide for the Care and Use of Laboratory Animals by the Institute of Animal Resources.

A male, 10-week-old NOD/Shi-*scid*/IL-2γ^{null} (NOG) immunodeficiency mouse was intubated and ventilated mechanically under general anesthesia with 2% isoflurane. Myocardial infarction was generated by ligating the left anterior descending artery with 8-0 Prolene (Ethicon, cat. no. EP8730H). 1.0×10^6 purified iPSC-CMs in 20 μL IMDM (Life Technologies, cat. no. 12440-053) were injected directly into the mouse heart by a Hamilton syringe with a 30-gauge needle. We transplanted iPSC-CMs differentiated from 201B7-luc iPSCs, which continuously express luciferase. To confirm the engraftment of iPSC-CMs, bioluminescence imaging was conducted. Mice were anesthetized with inhaled isoflurane, and D-luciferin (SPI, cat.no. XLF-1) was administered at a dose of 200 mg/kg i.p.

Images of the mice were captured using an in vivo bioluminescence imaging system (IVIS, Caliper Life Sciences). In the control mice, 20 μL IMDM alone was injected.

Before surgery and every two weeks thereafter, the mice were mildly anesthetized with inhaled isoflurane, and their left-ventricular dimensions (LVDd and LVDs) were measured using transthoracic echocardiography (GE Vivid S, GE). The fractional shortening (FS) was calculated as 100×(LVDd-LVDs) / LVDd (%) as an index of cardiac function.

Immunostaining and flow cytometry

Immunostaining was performed using the following primary antibodies: rabbit anti-cardiac Troponin T (abcam, cat. no. ab45932; 1:400), mouse anti-cardiac Troponin T (Thermo Scientific, cat. no. MS-295-P; 1:200), goat anti-luciferase (Promega, cat. no. G7451; 1:100), rabbit anti-MLC2V (Proteintech, cat. no. 10906-1-AP; 1:500), mouse anti-COUTPF-Ⅱ (R&D Systems, cat. no. PP-H7147-00; 1:200), rabbit anti-NKX2.5 (Cell Signaling Technology, cat. no. 8792; 1:800), rabbit anti-Chromogranin A (Abcam, cat. no. ab68271, 1:500), rat anti-C-peptide (DSHB, cat. no. GN-ID4, 1:200), mouse anti-glucagon (Sigma-Aldrich, cat. no. G2654; 1:200), rabbit anti-somatostatin (Dako, cat. no. A0566: 1:200), and goat anti-PDX1 (R&D Systems, cat. no. AF2419; 1:200). The secondary antibodies used in this study were as follows: goat anti-mouse IgG-Alexa Fluor 546 (Life Technologies, cat. no. A-11030; 1:400), goat anti-rabbit IgG-Alexa Fluor 488 (Life Technologies, cat. no. A-11034; 1:400), donkey anti-rabbit IgG-Alexa Fluor 488 (Life Technologies, cat. no. A-21206; 1:400), donkey anti-mouse IgG-Alexa Fluor 546 (Life Technologies, cat. no. A-10036; 1:400), donkey anti-rat IgG-Alexa Fluor 647 (Jackson, cat. no. 712-605-150; 1:400), donkey anti-goat IgG-Alexa Fluor 488 (Life Technologies, cat. no. A-11055; 1:400). Hoechst 33342 (Life Technologies, cat. no. H3570; 1:10000) was used to counterstain nuclei. The stained cells were visualized using a confocal microscope (FV1000, Olympus).

For the preparation of flow cytometer samples, we used the following antibodies: APC mouse anti-human CD4 (BD Biosciences, cat. no. 340443; 1:100), APC mouse anti-human CD31 (Biolegend, cat. no. 303116; 1:30), Alexa Fluor 647 mouse anti-human CD49a (Biolegend, cat. no. 328310; 1:20), APC mouse anti-human CD90 (BD Pharmingen, cat. no. 559869; 1:50), APC mouse anti-human CD140b (Biolegend cat. no. 323608; 1:10) PE/Cy7 mouse anti-human CD172a/b (Biolegend, cat. no. 323808; 1:20), mouse anti-cardiac Troponin T (Thermo Scientific, cat. no. MS-295-P; 1:200), and APC goat anti-mouse IgG (BD Biosciences, cat. no. 550826; 1:100). APC mouse IgG1 k isotype control (BD pharmingen, cat. no. 554681; 1:50) and PE/Cy7 mouse IgG1 k isotype control (BD pharmingen, cat. no. 557872; 1:50) were used as controls.

To measure the proportion of CMs, staining was carried out on cells fixed with 4% paraformaldehyde in PBS and done in PBS with 2% FCS and 0.5% saponin (Sigma, cat. no. 84510). Stained cells were analyzed and sorted using FACSAria II (BD Biosciences). Data were analyzed using FlowJo v10.6.1 analysis software (BD Biosciences).

Recording action potentials

To record action potentials, 2×10^5 iPSC-CMs were placed on a 35-m glass bottom dish, and the medium was exchanged with Gey's Balanced Salt Solution (Sigma-Aldrich, cat. no. G9779) and 0.1% Fluo Volt (Thermo Fisher Scientific, cat. no. F10488), which is a voltage-sensitive fluorescent probe. After 20 minutes of incubation at 37℃, the medium was exchanged with Gey's Balanced Salt Solution without Fluo Volt, and the sample was incubated for another hour at 37℃. Thereafter, the action potentials were recorded using AquaCosmos software (Hamamatsu Photonics). The recordings were performed under electrical stimulation at 1 Hz by Master-9 (AMPI) in the ventricular and atrial protocols, and under spontaneous beating condition in the nodal protocol.

Quantitative PCR

Total RNA was extracted using RNeasy Mini Kit (QIAGEN) after lysing the cells with QIAzol Lysis Reagent (QIAGEN). Extracted RNA was reverse transcribed into cDNA using ReverTra Ace qPCR RT Master Mix with gDNA Remover (TOYOBO). A qPCR analysis was performed with TaqMan probes (Thermo Fisher Scientific). The samples were analyzed using StepOnePlus Real-Time PCR System (Applied Biosystems). The fold change of the gene expressions was calculated using the ddCt method. The TaqMan probes were GAPDH (Assay ID; Hs99999905_m1), MYL2 (Assay ID; Hs00166405_m1), IRX4 (Assay ID; Hs00212560_m1), MYL7 (Assay ID; Hs01085598_g1), NR2F2 (COUPTF-Ⅱ) (Assay ID; Hs00819630_m1), SHOX2 (Assay ID; Hs01061127_m1), and ISL1 (Assay ID;Hs00158126_m1).

Supplemental references

Hatani, T., Miki, K., and Yoshida, Y. (2018). Induction of Human Induced Pluripotent Stem Cells to Cardiomyocytes Using Embryoid Bodies. Methods in molecular biology (Clifton, N.J.) *1816*, 79-92. 10.1007/978-1-4939-8597-5_6.

Kimura, A., Toyoda, T., Nishi, Y., Nasu, M., Ohta, A., and Osafune, K. (2017). Small molecule AT7867 proliferates PDX1-expressing pancreatic progenitor cells derived from human pluripotent stem cells. Stem Cell Res *24*, 61-68. 10.1016/j.scr.2017.08.010.

Toyoda, T., Mae, S., Tanaka, H., Kondo, Y., Funato, M., Hosokawa, Y., Sudo, T., Kawaguchi, Y., and Osafune, K. (2015). Cell aggregation optimizes the differentiation of human ESCs and iPSCs into pancreatic bud-like progenitor cells. Stem Cell Res *14*, 185-197. 10.1016/j.scr.2015.01.007.

	Name	sequence (5' to 3')
CD4-ORF		
Primer	CD4-ORF-Fwd	CACCGGTCGCCACCATGAACCGGGGAGTCCCTTTTAG
	CD4-ORF-Rev	GCCCCGCAGAAGGTCTAGACTAGTGCCGGCACCTGACACAG
Template	pMACS 4.1 (Miltenyi Biotec, cat. no. 130-091-886)	
CD271-ORF		
Primer	LNGFR-ORF-Fwd	CACCGGTCGCCACCATGGGGGCAGGTGCCACCGGCC
	LNGFR-ORF-Rev	GCCCCGCAGAAGGTCTAGACTACCTCTTGAAGCTATGTAG
Template	pMACS LNGFR (Miltenyi Biotec, cat. no. 130-091-890)	
BFP-ORF		
Primer	FwdtagBFP	CACCGGTCGCCACCATGGGATCCAGCGAG
	RevtagBFP	GCCCCGCAGAAGGTCTAGACTATCACTCGAGATGCATATGAGATC
Template	pAM-tagBFP (Miki *et al.*, 2015)	
***PAC*-ORF**		
Primer	Fwd*PAC*	CACCGGTCGCCACCATGACCGAGTACAAGCCCACG
	Rev*PAC*	GCCCCGCAGAAGGTCTAGCTCAGGCACCGGGCTTGC
Template	pPyCAG-Nanog-IP (Addgene, cat. no. 13838)	
Bim-ORF		
Primer	FwdBim	CACCGGTCGCCACCATG
	RevBim	GCCCCGCAGAAGGTCTAGAATCAATGCATTCTCCACACCAG
Template	pUC19_hBimELwoT7	
5'UTR		
Primer	T7FwdG3C	CAGTGAATTGTAATACGACTCACTATAGGGC

	Rev5UTR	CATGGTGGCGACCGGTGTCTTATATTTCTTCTTACTC
Template	temp5UTR	CAGTGAATTGTAATACGACTCACTATAGGGCGAATTAAGAGAGAAAAGAAGAGTAAGAAGAAAT ATAAGACACCGGTCGCCACCATG
3'UTR		
Primer	Fwd3UTR	TCTAGACCTTCTGCGGGGC
	Rev3UTR	TTTTTTTTTTTTTTTTTTTTCCTACTCAGGCTTTATTCAAAGACCAAG
Template	temp3UTR	TCTAGACCTTCTGCGGGGCTTGCCTTCTGGCCATGCCCTTCTTCTCTCCCTTGCACCTGTACCT CTTGGTCTTTGAATAAAGCCTGAGTAGG
mRNA		
Primer	T7FwdG3C	GCTAATACGACTCACTATAGGTTCCTTAATCGCGGATCC
	Rev120A	TTTTTTTTTTTTTTTTTTTTTTTTTTTTTTTTTTTTTTTTTTTTTTTTTTTTTTTTTTTTTTTT TTTTTTTTTTTTTTTTTTTTTTTTTTTTTTTTTTTTTTTTTTTTTTTTTTTTTTTTTCCTACTCAGG CTTTATTCA
Template	5'UTR product (above)	
	ORF product (above)	
	3'UTR product (above)	
complete sequence		

	BFP-mRNA	CAGTGAATTGTAATACGACTCACTATAGGGCGAATTAAGAGAGAAAAGAAGAGTAAGAAGAAAT ATAAGACACCGGTCGCCACCATGGGATCCAGCGAGCTGATTAAGGAGAACATGCACATGAAGCT GTACATGGAGGGCACCGTGGACAACCATCACTTCAAGTGCACATCCGAGGGCGAAGGCAAGCCC TACGAGGGCACCCAGACCATGAGAATCAAGGTGGTCGAGGGCGGCCCTCTCCCCTTCGCCTTC GACATCCTGGCTACTAGCTTCCTCTACGGCAGCAAGACCTTCATCAACCACACCCAGGGCATCC CCGACTTCTTCAAGCAGTCCTTCCCTGAGGGCTTCACATGGGAGAGAGTCACCACATACGAAGA CGGGGGCGTGCTGACCGCTACCCAGGACACCAGCCTCCAGGACGGCTGCCTCATCTACAACGTC AAGATCAGAGGGGTGAACTTCACATCCAACGGCCCTGTGATGCAGAAGAAAACACTCGGCTGGG AGGCCTTCACCGAGACGCTGTACCCCGCTGACGGCGGCCTGGAAGGCAGAAACGACATGGCCC TGAAGCTCGTGGGCGGGAGCCATCTGATCGCAAACATCAAGACCACATATAGATCCAAGAAACC CGCTAAGAACCTCAAGATGCCTGGCGTCTACTATGTGGACTACAGACTGGAAAGAATCAAGGAG GCCAACAACGAGACCTACGTCGAGCAGCACGAGGTGGCAGTGGCCAGATACTGCGACCTCCCTA GCAAACTGGGGCACAAGCTTAATAGATCTCATATGCATCTCGAGTGATAGTCTAGACCTTCTGC GGGGCTTGCCTTCTGGCCATGCCCTTCTTCTCTCCCTTGCACCTGTACCTCTTGGTCTTTGAAT AAAGCCTGAGTAGGAAAAAAAAAAAAAAAAAAAAAAAAAAAAAAAAAAAAAAAAAAAAAAAAA AAAAAAAAAAAAAAAAAAAAAAAAAAAAAAAAAAAAAAAAAAAAAAAAAAAAAAAAAAAAAA A

	CD4-mRNA	CAGTGAATTGTAATACGACTCACTATAGGGCGAATTAAGAGAGAAAAGAAGAGTAAGAAGAAAT ATAAGACACCGGTCGCCACCATGAACCGGGGAGTCCCTTTTAGGCACTTGCTTCTGGTGCTGCA ACTGGCGCTCCTCCCAGCAGCCTACTCAGGGAAAGAAAGTGGTGCTGGGCAAAAAAGGGGATAC AGTGGAACTGACCTGTACAGCTTCCCAGAAGAAGAGCATACAATTCCACTGGAAAAACTCCAACC AGATAAAGATTCTGGGAAATCAGGGCTCCTTCTTAACTAAAGGTCCATCCAAGCTGAATGATCG CGCTGACTCAAGAAGAAGCCTTTGGGACCAAGGAAACTTCCCCCTGATCATCAAGAATCTTAAG ATAGAAGACTCAGATACTTACATCTGTGAAGTGGAGGACCAGAAGGAGGAGGTGCAATTGCTAG TGTTCGGATTGACTGCCAACTCTGACACCCACCTGCTTCAGGGGCAGAGCCTGACCCTGACCTT GGAGAGCCCCCCTGGTAGTAGCCCCTCAGTGCAATGTAGGAGTCCAAGGGGTAAAAACATACAG GGGGGGAAGACCCTCTCCGTGTCTCAGCTGGAGCTCCAGGATAGTGGCACCTGGACATGCACT GTCTTGCAGAACCAGAAGAAGGTGGAGTTCAAAATAGACATCGTGGTGCTAGCTTTCCAGAAGG CCTCCAGCATAGTCTATAAGAAAGAGGGGGAACAGGTGGAGTTCTCCTTCCCACTCGCCTTTAC AGTTGAAAAGCTGACGGGCAGTGGCGAGCTGTGGTGGCAGGCGGAGAGGGCTTCCTCCTCCAA GTCTTGGATCACCTTTGACCTGAAGAACAAGGAAGTGTCTGTAAAATGGGTTACCCAGGACCCT AAGCTCCAGATGGGCAAGAAGCTCCCGCTCCACCTCACCCTGCCCCAGGCCTTGCCTCAGTATG CTGGCTCTGGAAACCTCACCCTGGCCCTTGAAGCGAAAACAGGAAAGTGCATCAGGAAGTGAAC CTGGTGGTGATGAGAGCCACTCAGCTCCAGAAAAATTTGACCTGTGAGGTGTGGGGACCCACC TCCCCTAAGCTGATGCTGAGCTTGAAACTGGAGAACAAGGAGGCAAAGGTCTCGAAGCGGGAG AAGGCGGTGTGGGTGCTGAACCCTGAGGCGGGGATGTGGCAGTGTCTGCTGAGTGACTCGGG ACAGGTCCTGCTGGAATCCAACATCAAGGTTCTGCCCACATGGTCGACCCCGGTGCAGCCAATG GCCCTGATTGTGCTGGGGGGCGTCGCCGGCCTCCTGCTTTTCATTGGGCTAGGCATCTTCTTC TGTGTCAGGTGCCGGCACTAGTCTAGACCTTCTGCGGGGCTTGCCTTCTGGCCATGCCCTTCT TCTCTCCCTTGCACCTGTACCTCTTGGTCTTTGAATAAAGCCTGAGTAGGAAAAAAAAAAAAAA AAAAAAAAAAAAAAAAAAAAAAAAAAAAAAAAAAAAAAAAAAAAAAAAAAAAAAAAAAAAAAA AAAAAAAAAAAAAAAAAAAAAAAAAAAAAAAAAAA

	PAC-mRNA	CAGTGAATTGTAATACGACTCACTATAGGGCGAATTAAGAGAGAAAAGAAGAGTAAGAAGAAAT ATAAGACACCGGTCGCCACCATGACCGAGTACAAGCCCACGGTGCGCCTCGCCACCCGCGACGA CGTCCCCAGGGCCGTACGCACCCTCGCCGCCGCGTTCGCCGACTACCCCGCCACGCGCCACACC GTCGATCCGGACCGCCACATCGAGCGGGTCACCGAGCTGCAAGAACTCTTCCTCACGCGCGTCG GGCTCGACATCGGCAAGGTGTGGGTCGCGGACGACGGCGCCGCGGTGGCGGTCTGGACCACG CCGGAGAGCGTCGAAGCGGGGGCGGTGTTCGCCGAGATCGGCCCGCGCATGGCCGAGTTGAG CGGTTCCCGGCTGGCCGCGCAGCAACAGATGGAAGGCCTCCTGGCGCCGCACCGGCCCAAGGA GCCCGCGTGGTTCCTGGCCACCGTCGGCGTCTCGCCCGACCACCAGGGCAAGGGTCTGGGCAG CGCCGTCGTGCTCCCCGGAGTGGAGGCGGCCGAGCGCGCCGGGGTGCCCGCCTTCCTGGAGA CCTCCGCGCCCCGCAACCTCCCCTTCTACGAGCGGCTCGGCTTCACCGTCACCGCCGACGTCGA GGTGCCCGAAGGACCGCGCACCTGGTGCATGACCCGCAAGCCCGGTGCCTGAGTCTAGACCTT CTGCGGGGCTTGCCTTCTGGCCATGCCCTTCTTCTCTCCCTTGCACCTGTACCTCTTGGTCTTT GAATAAAGCCTGAGTAGGAAAAAAAAAAAAAAAAAAAAAAAAAAAAAAAAAAAAAAAAAAAAA AAAAAAAAAAAAAAAAAAAAAAAAAAAAAAAAAAAAAAAAAAAAAAAAAAAAAAAAAAAAAA AAAAA
miRNA switch		
Primer	T7FwdB	CGACTCACTATAGGTTCCGCGATCGCGGATCCACAAGCTTTTTGCTCGTCTTATAGATCACACC GGTCGCCACCATG
	Rev120A	TTTTTTTTTTTTTTTTTTTTTTTTTTTTTTTTTTTTTTTTTTTTTTTTTTTTTTTTTTTTTTT TTTTTTTTTTTTTTTTTTTTTTTTTTTTTTTTTTTTTTTTTTTTTTTTTTCCTACTCAGG CTTTATTCA
Template	5UTRtemp_Txxx (below)	
	ORF product (above)	
	3'UTR product (above)	
Template oligo DNAs for miRNA switch		
	5UTRtemp_T208a	CGACTCACTATAGGTTCCGCGATCGCGGATCCACAAGCTTTTTGCTCGTCTTATAGATCACACC GGTCGCCACCATG

	5UTRtemp_T375	CGACTCACTATAGGTTCCGCGATCGCGGATCCTCACGCGAGCCGAACGAACAAAAGATCACACC GGTCGCCACCATG
complete sequence		
	miR-208a-CD4 switch	GCTAATACGACTCACTATAGGTTCCTTAATCGCGGATCCACAAGCTTTTTGCTCGTCTTATAGA TCACACCGGTCGCCACCATGAACCGGGGAGTCCCTTTTAGGCACTTGCTTCTGGTGCTGCAACT GGCGCTCCTCCCAGCAGCCTACTCAGGGAAAGAAAGTGGTGCTGGGCAAAAAAGGGGATACAG TGGAACTGACCTGTACAGCTTCCCAGAAGAAGAGCATACAATTCCACTGGAAAAACTCCAACCAG ATAAAGATTCTGGGAAATCAGGGCTCCTTCTTAACTAAAGGTCCATCCAAGCTGAATGATCGCG CTGACTCAAGAAGAAGCCTTTGGGACCAAGGAAACTTCCCCCTGATCATCAAGAATCTTAAGATA GAAGACTCAGATACTTACATCTGTGAAGTGGAGGACCAGAAGGAGGAGGTGCAATTGCTAGTGT TCGGATTGACTGCCAACTCTGACACCCACCTGCTTCAGGGGCAGAGCCTGACCCTGACCTTGGA GAGCCCCCCTGGTAGTAGCCCCTCAGTGCAATGTAGGAGTCCAAGGGGTAAAAACATACAGGGG GGGAAGACCCTCTCCGTGTCTCAGCTGGAGCTCCAGGATAGTGGCACCTGGACATGCACTGTC TTGCAGAACCAGAAGAAGGTGGAGTTCAAAATAGACATCGTGGTGCTAGCTTTCCAGAAGGCCT CCAGCATAGTCTATAAGAAAGAGGGGGAACAGGTGGAGTTCTCCTTCCCACTCGCCTTTACAGT TGAAAAGCTGACGGGCAGTGGCGAGCTGTGGTGGCAGGCGGAGAGGGCTTCCTCCTCCAAGTC TTGGATCACCTTTGACCTGAAGAACAAGGAAGTGTCTGTAAAATGGGTTACCCAGGACCCTAAG CTCCAGATGGGCAAGAAGCTCCCGCTCCACCTCACCCTGCCCCAGGCCTTGCCTCAGTATGCTG GCTCTGGAAACCTCACCCTGGCCCTTGAAGCGAAAACAGGAAAGTGCATCAGGAAGTGAACCTG GTGGTGATGAGAGCCACTCAGCTCCAGAAAAATTTGACCTGTGAGGTGTGGGGACCCACCTCCC CTAAGCTGATGCTGAGCTTGAAACTGGAGAACAAGGAGGCAAAGGTCTCGAAGCGGGAGAAGG CGGTGTGGGTGCTGAACCCTGAGGCGGGGATGTGGCAGTGTCTGCTGAGTGACTCGGGACAG GTCCTGCTGGAATCCAACATCAAGGTTCTGCCCACATGGTCGACCCCGGTGCAGCCAATGGCCC TGATTGTGCTGGGGGGCGTCGCCGGCCTCCTGCTTTTCATTGGGCTAGGCATCTTCTTCTGTG TCAGGTGCCGGCACTAGTCTAGACCTTCTGCGGGGCTTGCCTTCTGGCCATGCCCTTCTTCTCT CCCTTGCACCTGTACCTCTTGGTCTTTGAATAAAGCCTGAGTAGGAAAAAAAAAAAAAAAAAAA AAAAAAAAAAAAAAAAAAAAAAAAAAAAAAAAAAAAAAAAAAAAAAAAAAAAAAAAAAAAAAA AAAAAAAAAAAAAAAAAAAAAAAAAAAAAA

	miR-208a-CD271 switch	GCTAATACGACTCACTATAGGTTCCTTAATCGCGGATCCACAAGCTTTTTGCTCGTCTTATAGA TCACACCGGTCGCCACCATGGGGGCAGGTGCCACCGGCCGCGCCATGGACGGGCCGCGCCTGC TGCTGTTGCTGCTTCTGGGGGTGTCCCTTGGAGGTGCCAAGGAGGCATGCCCCACAGGCCTGT ACACACACAGCGGTGAGTGCTGCAAAGCCTGAACCTGGGCGAGGGTGTGGCCCAGCCTTGTGG AGCCAACCAGACCGTGTGTGAGCCCTGCCTGGACAGCGTGACGTTCTCCGACGTGGTGAGCGC GACCGAGCCGTGCAAGCCGTGCACCGAGTGCGTGGGGCTCCAGAGCATGTCGGCGCCGTGCGT GGAGGCCGACGACGCCGTGTGCCGCTGCGCCTACGGCTACTACCAGGATGAGACGACTGGGCG CTGGAGGCGTGCCGCGTGTGCGAGGCGGGCTCGGGCCTCGTGTTCTCCTGCCAGGACAAGCAG AACACCGTGTGCGAGGAGTGCCCCGACGGCACGTATTCCGACGAGGCCAACCACGTGGACCCG TGCCTGCCCTGCACCGTGTGCGAGGACACCGAGCGCCAGCTCCGCGAGTGCACACGCTGGGCC GACGCCGAGTGCGAGGAGATCCCTGGCCGTTGGATTACACGGTCCACACCCCCAGAGGGCTCG GACAGCACAGCCCCCAGCACCCAGGAGCCTGAGGCACCTCCAGAACAAGAGCTCATAGCCAGCA CGGTGGCAGGTGTGGTGACCACAGTGATGGGCAGCTCCCAGCCCGTGGTGACCCGAGGCACAC CGACAACCTCATCCCTGTCTATTGCTCCATCCTGGCTGCTGTGGTTGTGGGTCTTGTGGCCTAC ATAGCCTTCAAGAGGTAGTCTAGACCTTCTGCGGGGCTTGCCTTCTGGCCATGCCCTTCTTCTC TCCCTTGCACCTGTACCTCTGGTCTTTGAATAAAGCCTGAGTAGGAAAAAAAAAAAAAAAAAAA AAAAAAAAAAAAAAAAAAAAAAAAAAAAAAAAAAAAAAAAAAAAAAAAAAAAAAAAAAAAAAA AAAAAAAAAAAAAAAAAAAAAAAAAAAAAA

	miR-375-CD4 switch	GCTAATACGACTCACTATAGGTTCCTTAATCGCGGATCCTCACGCGAGCCGAACGAACAAAAGA TCACACCGGTCGCCACCATGAACCGGGGAGTCCCTTTTAGGCACTTGCTTCTGGTGCTGCAACT GGCGCTCCTCCCAGCAGCCTACTCAGGGAAAGAAAGTGGTGCTGGGCAAAAAAGGGGATACAG TGGAACTGACCTGTACAGCTTCCCAGAAGAAGAGCATACAATTCCACTGGAAAAACTCCAACCAG ATAAAGATTCTGGGAAATCAGGGCTCCTTCTTAACTAAAGGTCCATCCAAGCTGAATGATCGCG CTGACTCAAGAAGAAGCCTTTGGGACCAAGGAAACTTCCCCCTGATCATCAAGAATCTTAAGATA GAAGACTCAGATACTTACATCTGTGAAGTGGAGGACCAGAAGGAGGAGGTGCAATTGCTAGTGT TCGGATTGACTGCCAACTCTGACACCCACCTGCTTCAGGGGCAGAGCCTGACCCTGACCTTGGA GAGCCCCCCTGGTAGTAGCCCCTCAGTGCAATGTAGGAGTCCAAGGGGTAAAAACATACAGGGG GGGAAGACCCTCTCCGTGTCTCAGCTGGAGCTCCAGGATAGTGGCACCTGGACATGCACTGTC TTGCAGAACCAGAAGAAGGTGGAGTTCAAAATAGACATCGTGGTGCTAGCTTTCCAGAAGGCCT CCAGCATAGTCTATAAGAAAGAGGGGGAACAGGTGGAGTTCTCCTTCCCACTCGCCTTTACAGT TGAAAAGCTGACGGGCAGTGGCGAGCTGTGGTGGCAGGCGGAGAGGGCTTCCTCCTCCAAGTC TTGGATCACCTTTGACCTGAAGAACAAGGAAGTGTCTGTAAAATGGGTTACCCAGGACCCTAAG CTCCAGATGGGCAAGAAGCTCCCGCTCCACCTCACCCTGCCCCAGGCCTTGCCTCAGTATGCTG GCTCTGGAAACCTCACCCTGGCCCTTGAAGCGAAAACAGGAAAGTGCATCAGGAAGTGAACCTG GTGGTGATGAGAGCCACTCAGCTCCAGAAAAATTTGACCTGTGAGGTGTGGGGACCCACCTCCC CTAAGCTGATGCTGAGCTTGAAACTGGAGAACAAGGAGGCAAAGGTCTCGAAGCGGGAGAAGG CGGTGTGGGTGCTGAACCCTGAGGCGGGGATGTGGCAGTGTCTGCTGAGTGACTCGGGACAG GTCCTGCTGGAATCCAACATCAAGGTTCTGCCCACATGGTCGACCCCGGTGCAGCCAATGGCCC TGATTGTGCTGGGGGGCGTCGCCGGCCTCCTGCTTTTCATTGGGCTAGGCATCTTCTTCTGTG TCAGGTGCCGGCACTAGTCTAGACCTTCTGCGGGGCTTGCCTTCTGGCCATGCCCTTCTTCTCT CCCTTGCACCTGTACCTCTTGGTCTTTGAATAAAGCCTGAGTAGGAAAAAAAAAAAAAAAAAAA AAAAAAAAAAAAAAAAAAAAAAAAAAAAAAAAAAAAAAAAAAAAAAAAAAAAAAAAAAAAAAA AAAAAAAAAAAAAAAAAAAAAAAAAAAAAA